CHAPTER IV

RESULTS AND DISCUSSION

4.1 Physico-Chemical Characterization

In this study, HMS and functionalized HMSs with amino-, mercapto- and octyl- functional groups were synthesized by direct co-condensation method and grafting method, respectively. Dodecylamine and TEOS were used as organic template and silica precursor, respectively. APTES, MPTMS and dimethyloctylchlorosilane were used for amino-, mercapto- and octyl- groups single functionalized HMS (SF-HMS). Then organic template was removed by calcination for HMS and solvent extraction for functionalized HMSs (A-HMS, M-HMS and OD-HMS). After that, physico-chemical characteristics of synthesized HMSs were investigated comparing with PAC. Obtained data were combined with adsorption experiment results for study relationships between physico-chemical characteristics (crystalline structure, surface characteristics, hydrophilicity, surface charges, etc.) and adsorption capacities to describe adsorption phenomenon on the surfaces.

4.1.1 Pore Structure

Figure 4.1 presents the X-ray Powder Diffraction (XRD) pattern of synthesized HMSs. According to the XRD pattern, synthesized pristine HMS (pure silica HMS) exhibited a strong single diffraction peak at $2\theta = 2.22°$ and weak peak around 4.3° as an evidence of the hexagonal crystalline structure, although crystalline structure of prepared HMS was not complete hexagonal crystalline (comparing with other hexagonal crystalline silicate), which should show an XRD pattern consisting of (100), (110), (200) and (210) diffraction for the hexagonal array of typical HMS material. Octyl functional group grafted HMS (OD-HMS) also showed the strong peak at $2\theta = 2.15°$, and very weak peak at around 4.5°. For M-HMS and A-HMS, XRD pattern indicated that crystalline structure was lost by co-condensation method compared with pristine HMS result.
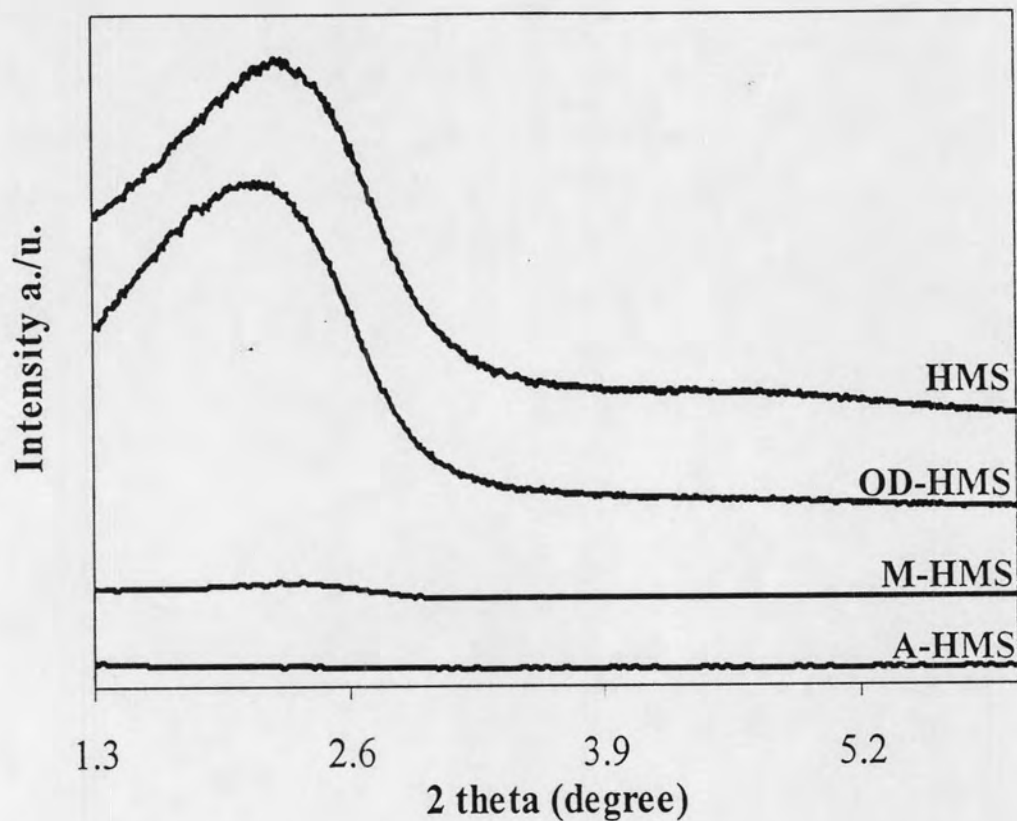
Figure 4.1 X-Ray Powder Diffraction patterns of synthesized HMSs

4.1.2 Surface Area and Pore Size

The Brunauer-Emmett-Teller (BET) method continues to be the most widely used method for the determination of surface area, pore volume and pore size distributions of porous materials from nitrogen adsorption-desorption isotherm data. The nitrogen adsorption-desorption isotherm (BET) were measured at 77 K on a Surface area and Porosity Analyzer. The BET equation can be represented in Equation 12 as shown below

$$\frac{p}{v(p_0 - p)} = \frac{1}{v_m c} + \frac{c-1}{v_m c} \frac{p}{p_0} \tag{12}$$

Where v = Volume of N_2 adsorbed by the sample under pressure p

p_0 = Saturated vapor pressure at the same temperature

v_m = Volume of N_2 adsorbed when the surface is covered with a unimolecular layer

c = Constant for a given adsorbate

The specific surface areas of samples were calculated from the adsorption data by Equation 13.

$$S = \frac{N_0 v_m A}{22414m} \qquad (13)$$

Where S = Specific surface area (m^2/g)

N_0 = Avogadro number

m = Amount of solid adsorbent (g)

A = Cross-section of the gas molecules (16.2 $A^{\circ 2}$ for N_2)

The Barrett-Joyner-Halenda (BJH) model was used for calculated of pore size distributions of materials.

The BET surface areas, pore volumes, and pore size distributions of HMS, functionalized HMSs and PAC were shown in Table 4.1.

Table 4.1 BET surface area, pore volume, and pore diameter of HMS, functionalized HMSs and PAC.

Adsorbents	Pore diameter (nm)	BET Surface Area (m²/g)	Pore volume (nm³/g)	Surface functional groups
HMS	2.60	712.24	773.42	Silanol
A-HMS	3.95	262.28	147.26	Amino
M-HMS	2.48	912.68	433.37	Mercapto
OD-HMS	2.36	476.56	499.00	Octyl
PAC	1.90	980.46	276.00	Carboxyl, Phenyl and others

The BET surface area of HMS, A-HMS, M-HMS, OD-HMS and PAC were found to be 712.24, 262.28, 912.68, 476.56 and 980.46 m²/g, respectively. The specific surface area of PAC was higher than other adsorbents that might cause highest adsorption capacity. Furthermore, the results showed that specific surface areas of organosilane functionalized HMSs were decreased due to increasing of amino functional group. Obviously, amino-functional groups considerably affect the structure of mesoporous silicate which was indicative of decrease of BET surface area. It was aforementioned in XRD patterns that it might be due to cross-link between amino-functional groups and silanol groups of silicates and conduct to weaker interaction between surfactant templates and silicate species. Opposing to amino-functional group, the specific surface area of M-HMS was larger than HMS, however XRD pattern of M-HMS shown the collapse of silicate structure significantly.

For pore size distribution, the average pore size of HMS, A-HMS, M-HMS, OD-HMS and PAC calculated by BJH model was 2.60, 3.95, 2.48, 2.36 and 1.90 nm, respectively. PAC had the smallest pore size in microporous structure. For HMS and functionalized HMSs, their average pore sizes were in the range of 2-50 nm which indicates that structure of adsorbents are mesoporous structures. However, presence of organo-functional groups on HMS affected to the average pore size. For example, mercaptopropyl groups on M-HMS exhibited a smaller pore size than

pristine HMS. However, A-HMS exhibited the larger average pore size than pristine HMS. It can be concluded that presence of amino-functional groups might deform hexagonal mesostructure which might cause increasing of average pore size.

4.1.3 Surface Functional Groups

Surface functional groups of pristine HMS and functionalized HMSs were investigated by Fourier Transform Infrared (FT-IR) Spectroscopy. It dealt with the vibration of chemical bonds in a molecule at various frequencies depending on the elements and types of bonds. In this experiment the FT-IR spectra was used to confirm functional groups on adsorbents surface which loaded during synthesis of functionalized HMSs. The FT-IR spectra of HMS and functionalized HMSs were showed in Figure 4.2-4.5.
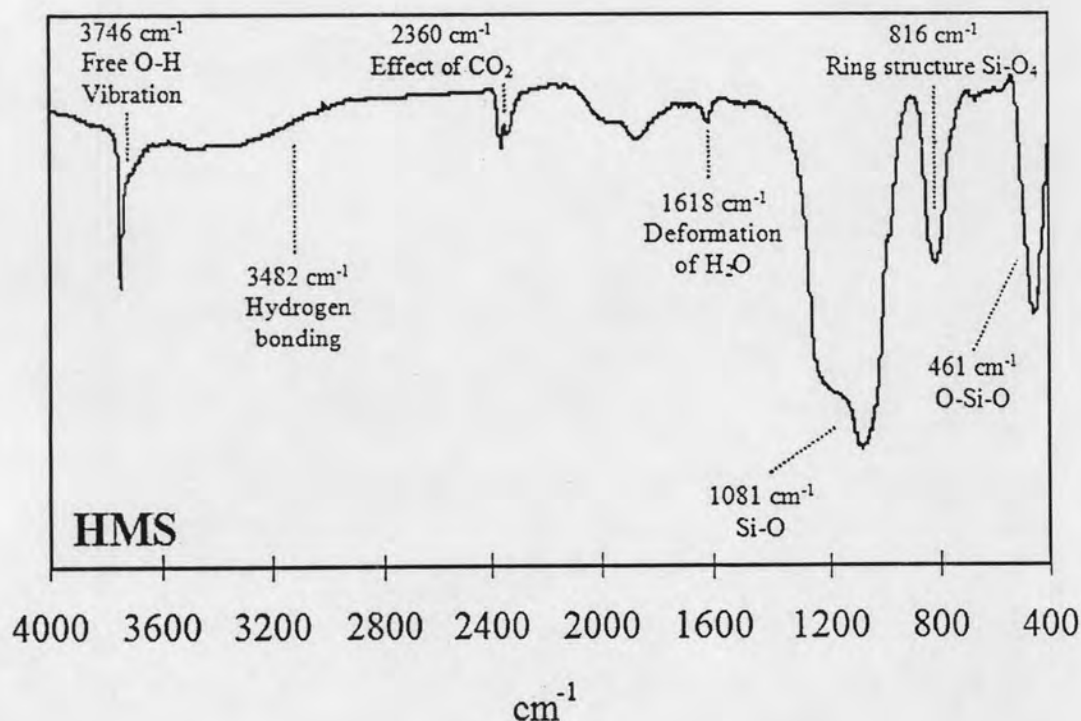
Figure 4.2 FT-IR spectra of HMS
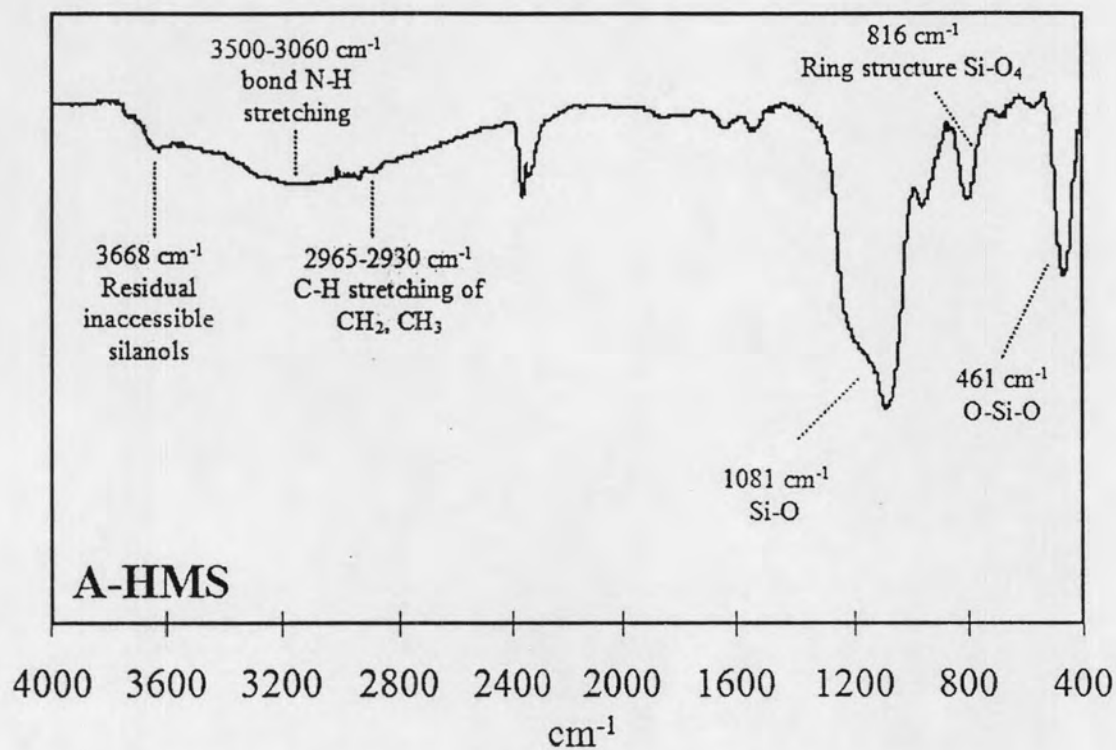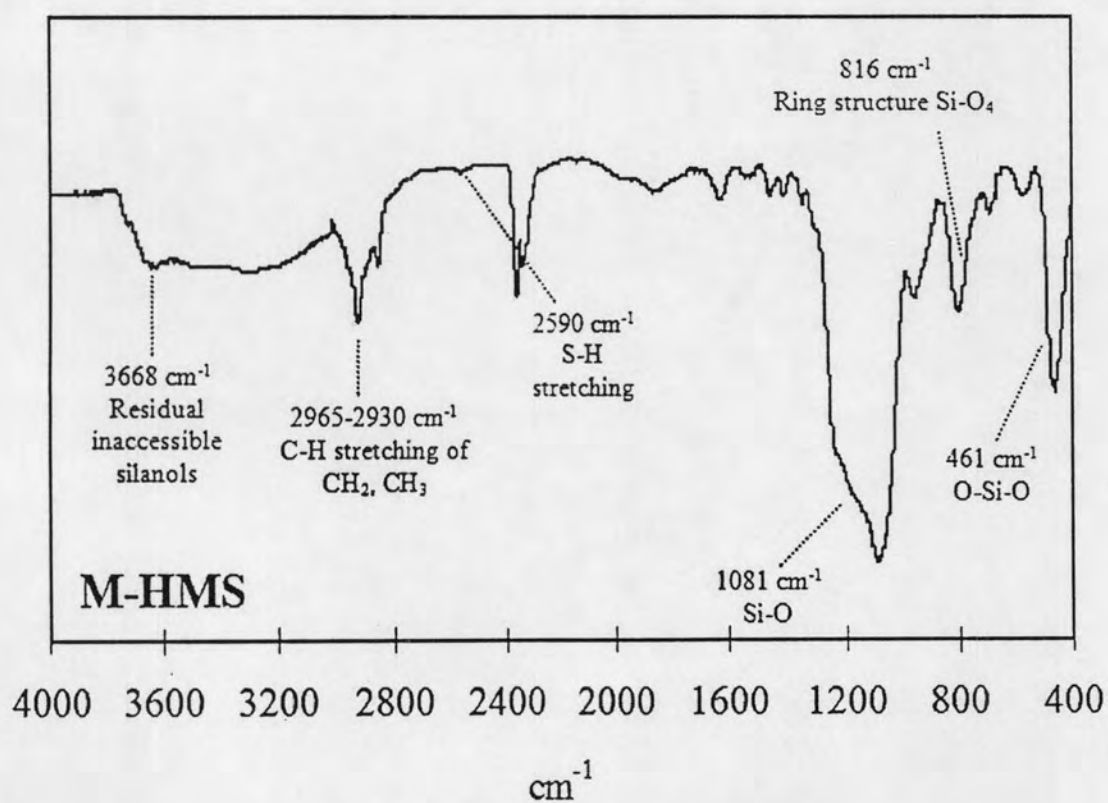
Figure 4.3 FT-IR spectra of A-HMS

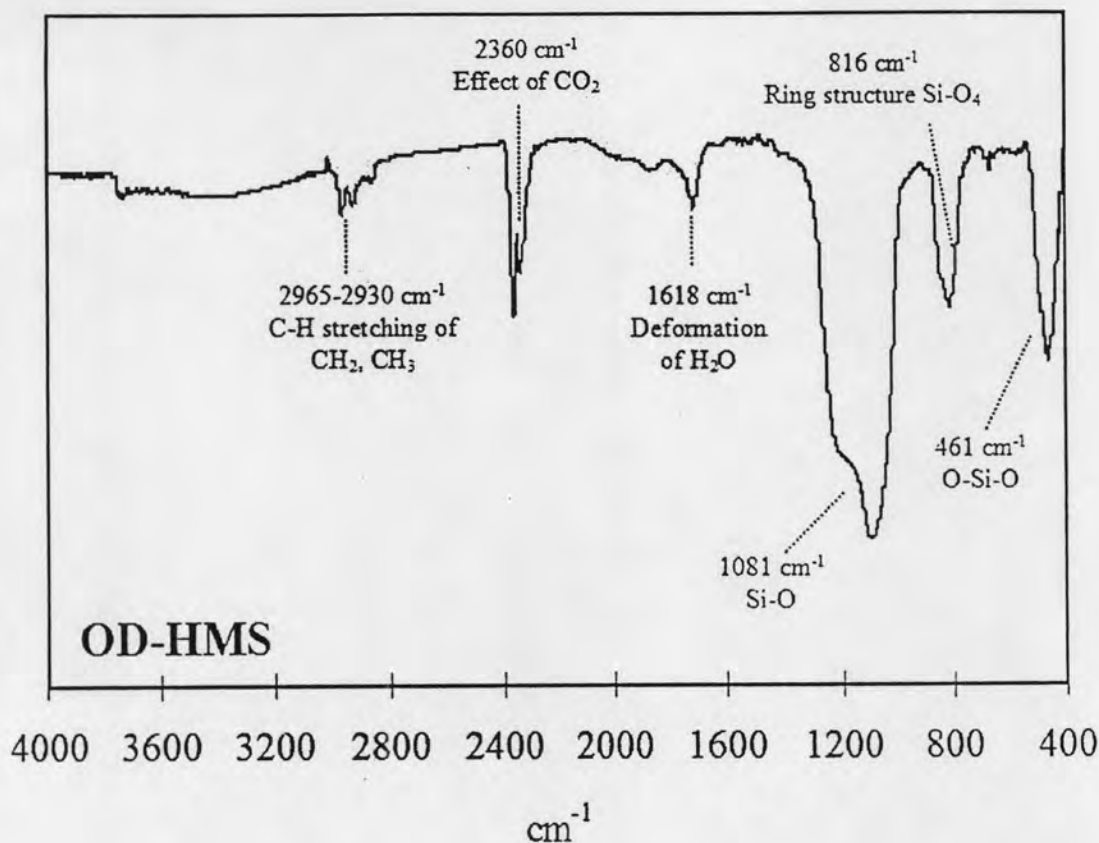**Figure 4.4** FT-IR spectra of M-HMS

Figure 4.5 FT-IR spectra of OD-HMS

All of the spectra gave evidences of Si-O-Si bonds by the adsorption peaks at around 470 cm^{-1}, 800 cm^{-1} and 1070 cm^{-1}. Sharp peak at 2360 cm^{-1} was caused by effect of CO_2 in air. The sharp peak at 3746 cm^{-1} of fresh HMS was due to the O-H stretching vibration of isolated non-hydrogen-bonded Si-OH. Broad tail of a peak at near 3482-3200 cm^{-1} was due to the hydrogen bonding of bonded hydroxyl groups. Moreover, very weak peak at 971 cm^{-1} was due to stretching mode vibration of Si-OH. The presence of silanol groups on HMS surface caused the hydrophilicity characteristic.

For functionalized HMSs, A-HMS had very weak peak at around 2930-2965 cm^{-1}, which evidences the presence of CH_2 and CH_3 functional group in 3-aminopropyltriethoxy structure. FT-IR spectrum of A-HMS also showed the peak at 3668 cm^{-1}, which were due to inaccessible silanol groups. However, peak of free N-H bonding of amino functional groups cannot be detected clearly because of broad peak

of hydrogen bonded N-H groups at 3500-3600 cm^{-1}. Hence, presence of amino functional groups was proved by TN detection method. However hydrophilicity of A-HMS can be confirmed by presence of peak at 3500-3600 cm^{-1}, which is due to hydrogen bonding of N-H functional groups.

FT-IR spectrum of M-HMS (Figure 4.4) confirmed the presence of grafted organic moieties results by peaks around 2930-2965 cm^{-1}. The peak of S-H functional group in M-HMS was a very weak peak (around 2590 cm^{-1}), but it can be used for proving the presence of S-H because there were not so many peaks of other functional groups around the peak of S-H functional groups. In addition, the peak detected at 3668 cm^{-1} was due to residual inaccessible silanol groups, which are inaccessible to 3-mercaptopropyl silylation reaction.

Figure 4.5 shows that OD-HMS had a group of peaks between 2930-2965 cm^{-1} due to C-H stretching of CH_2 and CH_3. Furthermore, drastic decreasing of peaks both free and bonded hydroxyl group at 3746 and 3482 cm^{-1} evidences significant increasing of hydrophobic characteristic of OD-HMS, which was caused by grafted organic functional groups. Hence, the presence of dimethyloctylchlorosilane functional groups on OD-HMS was confirmed.

4.1.4 Elemental Analysis

In addition to the evidence given by FT-IR spectra, amount of N and S in A-HMS and M-HMS were investigated for confirming the presence of N and S. Autoclave digestion by potassium per sulfate ($K_2S_2O_8$) in alkaline condition was conducted for quantitative nitrogen analysis. Inductively Coupled Plasma Optical Emission Spectroscopy (ICP-OES) technique was applied for S quantification. Pure silicate HMS was also investigated as a blank sample. Amount of N in A-HMS was quantified as 1.42%. S in M-HMS was detected as 9.90%. Obtained results and combination with FT-IR spectra of A-HMS and M-HMS can confirmed the presence of amino and mercapto functional groups on the surfaces of A-HMS and M-HMS, respectively.

Nitrogen content of A-HMS was found to be 1.42%, and the result shows sulfur content of M-HMS was found to be 9.90%. The results showed that

sulfur contents were nearly equal to amount of MPTMS loaded in synthesis process. It meant that mercapto-functional groups of MPTMS were not affected to reaction between surfactant templates and silica precursor, unlike amino-functional groups of APTES.
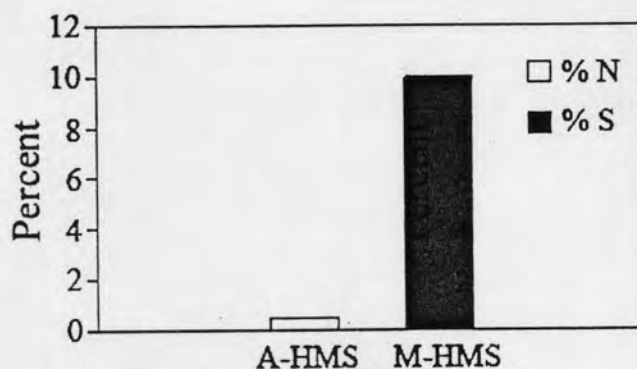

Figure 4.6 Total nitrogen and sulfur content in functionalized HMSs (%w/w)

4.1.5 Surface Charge

Acid/base titration technique was used to determine the surface charge of materials. The ionic strength was fixed at 0.01 M by NaOH solution. After equilibrium, pH of solutions were measured and plotted against surface charges. Surface charges were calculated from the principle of electro neutrality as shown in Equation 14.

$$\text{Surface charge (C/g)} = \{[HCl]_{add} - [NaOH]_{add} - [OH^-]\} \times 96500/W \quad (14)$$

Where $[HCl]_{add}$ = Concentration of HCl were added (mol/l)

$[NaOH]_{add}$ = Concentration of NaOH were added (mol/l)

$[H^+]$ = Concentration of proton (mol/l) calculated from pH = -log$[H^+]$

$[OH^-]$ = Concentration of hydroxide ion (mol/l) calculated from pOH = -log$[OH^-]$ and pOH = 14-pH

96500 = Faraday constant (C/mol)

W = Weight of adsorbent (g/l)

The surface charge density of HMS, A-HMS, M-HMS, OD-HMS, and PAC as function of pH were shown in Figure 4.7.
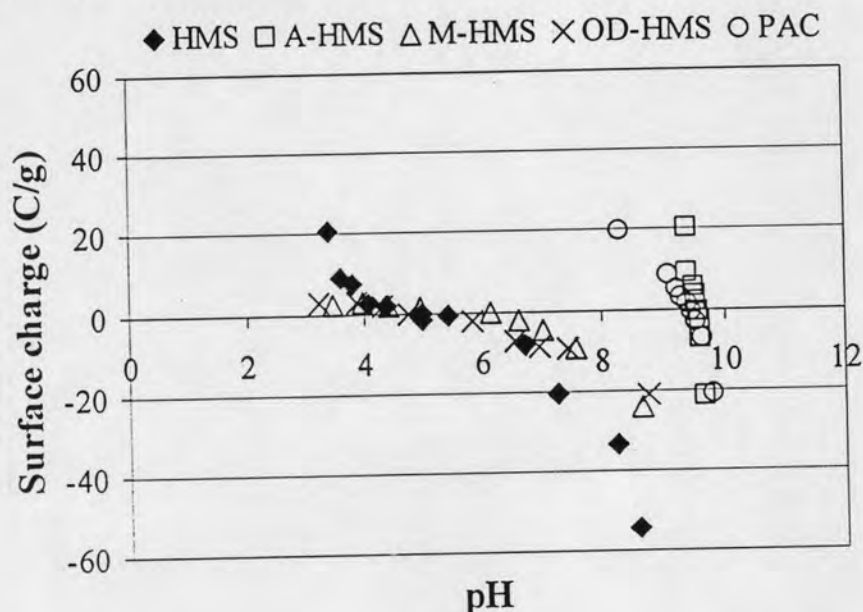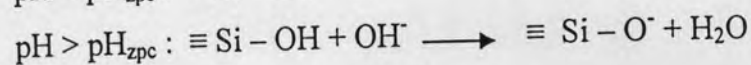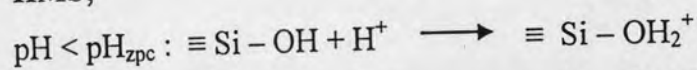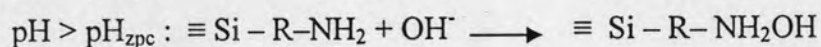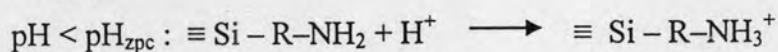
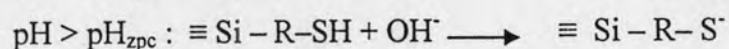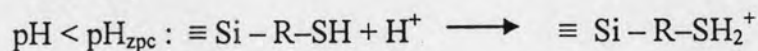◆ HMS ☐ A-HMS △ M-HMS ✕ OD-HMS ○ PAC

Figure 4.7 Surface charges of HMS, functionalized HMSs and PAC as a function of pH

Figure 4.7 showed the surface charge density of applied adsorbents as function of pH. The pH value that gives zero surface charge was defined as the zero point of charge (pH_{zpc}). pH_{zpc} of all adsorbents was summarized in Table 4.2.

At this pH value, the positive charge of cationic surface groups and the negative charge of anionic surface groups were balanced. As shown in figure 4.7, the surface charge density decreased as the pH increased from acidic region to neutral pH. The silanol groups on the surface of HMSs gain or lose protons, resulting in surface charge variation at different pH as shown in the following equation. At low pH, surface sites of HMSs were protonated and the surfaces become positively charged; whereas at a high pH, the surface hydroxides lose their protons, and the surface became negatively charged.

HMS;

$$pH < pH_{zpc} : \equiv Si - OH + H^+ \longrightarrow \equiv Si - OH_2^+$$
$$pH > pH_{zpc} : \equiv Si - OH + OH^- \longrightarrow \equiv Si - O^- + H_2O$$

A-HMS;

$pH < pH_{zpc}$: $\equiv Si - R\text{–}NH_2 + H^+ \longrightarrow \equiv Si - R\text{–}NH_3^+$

$pH > pH_{zpc}$: $\equiv Si - R\text{–}NH_2 + OH^- \longrightarrow \equiv Si - R\text{–}NH_2OH$

M-HMS;

$pH < pH_{zpc}$: $\equiv Si - R\text{–}SH + H^+ \longrightarrow \equiv Si - R\text{–}SH_2^+$

$pH > pH_{zpc}$: $\equiv Si - R\text{–}SH + OH^- \longrightarrow \equiv Si - R\text{–}S^-$

Table 4.2 pH_{zpc} of HMS, A-HMS, M-HMS, OD-HMS and PAC

Adsorbents	pH_{zpc}
HMS	5.5
A-HMS	9.5
M-HMS	6.2
OD-HMS	4.4
PAC	9.5

The amino-functional groups presented on HMS gave a higher pH_{zpc} than pristine HMS. The amino groups are protonated and become positive charges on surface. Furthermore, surface charge of M-HMS did not change significantly at pH in range of 4-6.

4.2 Adsorption Kinetic

The adsorption kinetic for Cd(II), Cu(II), methylene blue and TX-100 adsorption were performed by varying contact time from 0 to 24 h under batch condition at Cd(II), Cu(II), methylene blue and TX-100 concentration of 20, 20, 50 and 400 mg/L, respectively, and amount of adsorbents of 0.33 g/L. Exception of PAC was performed at methylene blue concentration of 230 mg/L. The pH of solution was fixed at pH 5 by 0.1 M of phosphate buffer. Samples were shaken in shaking water bath at 25°C, 150 rpm. The results were shown in Figure 4.8-4.11.

To analyze the adsorption rate of Cd(II), Cu(II), methylene blue and TX-100 onto HMS, functionalized HMSs and PAC, the pseudo-first-order equation of Lagergren and the pseudo-second-order rate were evaluated base on the experimental data. The pseudo-first-order and pseudo-second-order kinetic model are expressed as Equation 15 and Equation 16.

$$\ln(q_e - q_t) = \ln q_e - k_1 t \qquad (15)$$

$$\frac{t}{q_t} = \frac{1}{2k_2 q_e^2} + \frac{t}{q_e} \qquad (16)$$

Where k_1 = Lagergren rate constant (hr^{-1})

k_2 = Pseudo-second-order rate constant ($g\ mg^{-1}\ hr^{-1}$)

q_e = Amounts of pollutant sorbed at equilibrium (hr)

q_t = Amounts of pollutant sorbed at time t (hr)

The experimental data were plotted $\ln(q_e - q_t)$ versus time for first-order-rate and plotted t/q$_t$ versus time for second-order rate. The kinetic constants of adsorbents were calculated and listed in Table 4.3-4.6.

The adsorption kinetics of Cd(II) and Cu(II) were shown in Figure 4.8-4.9. All adsorbents reached equilibrium around 6 hr. M-HMS reached equilibrium first and followed by HMS. For adsorption kinetic of methylene blue in Figure 4.10, all adsorbents reached equilibrium around 4 hr., and PAC reached equilibrium first and followed by OD-HMS. Adsorption kinetic in Fig. 4.11 showed that TX-100 adsorption on HMSs took place as fast as PAC, and pristine HMS has the highest maximum adsorption capacity, followed by M-HMS.

It was found that the pseudo-second-order model can be fitted for adsorption of all pollutants onto every adsorbents indicated by the correlation coefficients comparing with pseudo-first-order model. It means the pseudo-second-order rate models could be described adsorption kinetics for Cd(II), Cu(II), methylene blue and TX-100 adsorption. Moreover, the experimental q_e values and the calculated q_e obtained from the linear plot in Eq. 16 were compared as shown in Table 4.3-4.6.

The results in Table 4.3-4.6 exhibit very good consistency between that calculated q_e and experimental q_e.

Table 4.3 Kinetics values calculated for Cd(II) adsorption onto HMS, functionalized HMSs, and PAC.

Adsorbent	Pseudo First Order		Pseudo Second Order		Calculated	Experimental	h
	R^2	k_1 (hr^{-1})	R^2	k_2 (g/mg hr)	q_e (mg/g)	q_e (mg/g)	(mg/g hr)
HMS	0.97	0.76	1.00	0.84	0.574	0.528	0.278
A-HMS	0.94	1.30	1.00	1.37	0.386	0.358	0.205
M-HMS	0.76	0.13	1.00	1.37	3.370	3.340	15.570
OD-HMS	0.98	0.46	1.00	0.43	0.757	0.672	0.248
PAC	0.76	-0.39	0.99	0.01	4.963	2.173	0.161

Table 4.4 Kinetics values calculated for Cu(II) adsorption onto HMS, functionalized HMSs, and PAC.

Adsorbent	Pseudo First Order		Pseudo Second Order		Calculated	Experimental	h
	R^2	k_1 (hr^{-1})	R^2	k_2 (g/mg hr)	q_e (mg/g)	q_e (mg/g)	(mg/g hr)
HMS	0.43	0.70	1.00	0.98	1.689	1.648	2.805
A-HMS	0.82	1.20	0.96	0.25	0.487	0.364	0.060
M-HMS	0.58	-1.43	1.00	0.21	19.548	19.349	79.181
OD-HMS	0.47	0.04	0.99	0.44	2.861	2.770	3.638
PAC	0.57	-0.48	1.00	0.72	10.114	10.057	74.016

Table 4.5 Kinetics values calculated for methylene blue adsorption onto HMS, functionalized HMSs, and PAC.

Adsorbent	Pseudo First Order		Pseudo Second Order		Calculated	Experimental	h
	R^2	k_1 (hr^{-1})	R^2	k_2 (g/mg hr)	q_e (mg/g)	q_e (mg/g)	(mg/g hr)
HMS	0.86	0.28	1.00	0.02	35.316	32.806	1,244.37
A-HMS	0.72	0.25	1.00	0.11	8.694	8.317	75.24
M-HMS	0.66	0.36	1.00	0.04	89.221	88.252	7,958.71
OD-HMS	0.38	0.42	1.00	0.38	81.240	81.130	6,599.99
PAC	0.89	0.50	1.00	0.01	173.883	170.960	30,232.12

Table 4.6 Kinetics values calculated for TX-100 adsorption onto HMS, functionalized HMSs, and PAC.

Adsorbent	Pseudo First Order		Pseudo Second Order		Calculated	Experimental	h
	R^2	k_1 (hr^{-1})	R^2	k_2 (g/mg hr)	q_e (mg/g)	q_e (mg/g)	(mg/g hr)
HMS	0.96	8.33×10^{-4}	1.00	2.67×10^{-6}	18.950	18.668	21,543.99
A-HMS	0.74	1.67×10^{-4}	0.98	6.83×10^{-6}	1.441	1.335	121.80
M-HMS	0.76	6.67×10^{-4}	0.98	3.33×10^{-7}	12.656	10.397	9,430.12
OD-HMS	0.84	8.33×10^{-4}	0.93	1.67×10^{-7}	13.176	9.900	9,694.338
PAC	0.98	8.33×10^{-4}	1.00	2.33×10^{-6}	9.776	9.465	5,731.33

In addition, the initial adsorption rate can also be obtained from this model from Equation 17 showed in Table 4.3-4.6.

$$h = k_2 q_e^2 \qquad (17)$$

Where h is the initial adsorption rate (mg/g h). From calculations, it showed that M-HMS, PAC and HMS had the highest initial adsorption rate for Cd(II) and Cu(II) adsorption, methylene blue adsorption and TX-100 adsorption, respectively. The calculated data clearly agree with experimental data observed in Figure 4.8-4.11 that initial time, concentration of Cd(II), Cu(II), methylene blue and TX-100 adsorbed onto PAC rapidly decrease, and slowly decrease until equilibrium stage at 4-5 hr.

In table 4.3-4.6, the highest k_2 value found in A-HMS and M-HMS for Cd(II) adsorption kinetic. For Cu(II) adsorption kinetic found the highest in HMS. Moreover, in methylene blue and TX-100 adsorption kinetic got the highest in OD-HMS and A-HMS, respectively.

For Cd(II), Cu(II), MB and TX-100 adsorption kinetic, k_2 value got the lowest in PAC, M-HMS, PAC and OD-HMS, respectively. Thus, at the same adsorption rate, the lowest k_2 value meant the lowest k_2 value adsorbent can adsorbed pollutants greater than another adsorbents. Moreover, these results showed that using the lowest k_2 value adsorbent in small amount can adsorbed pollutants in high amount.
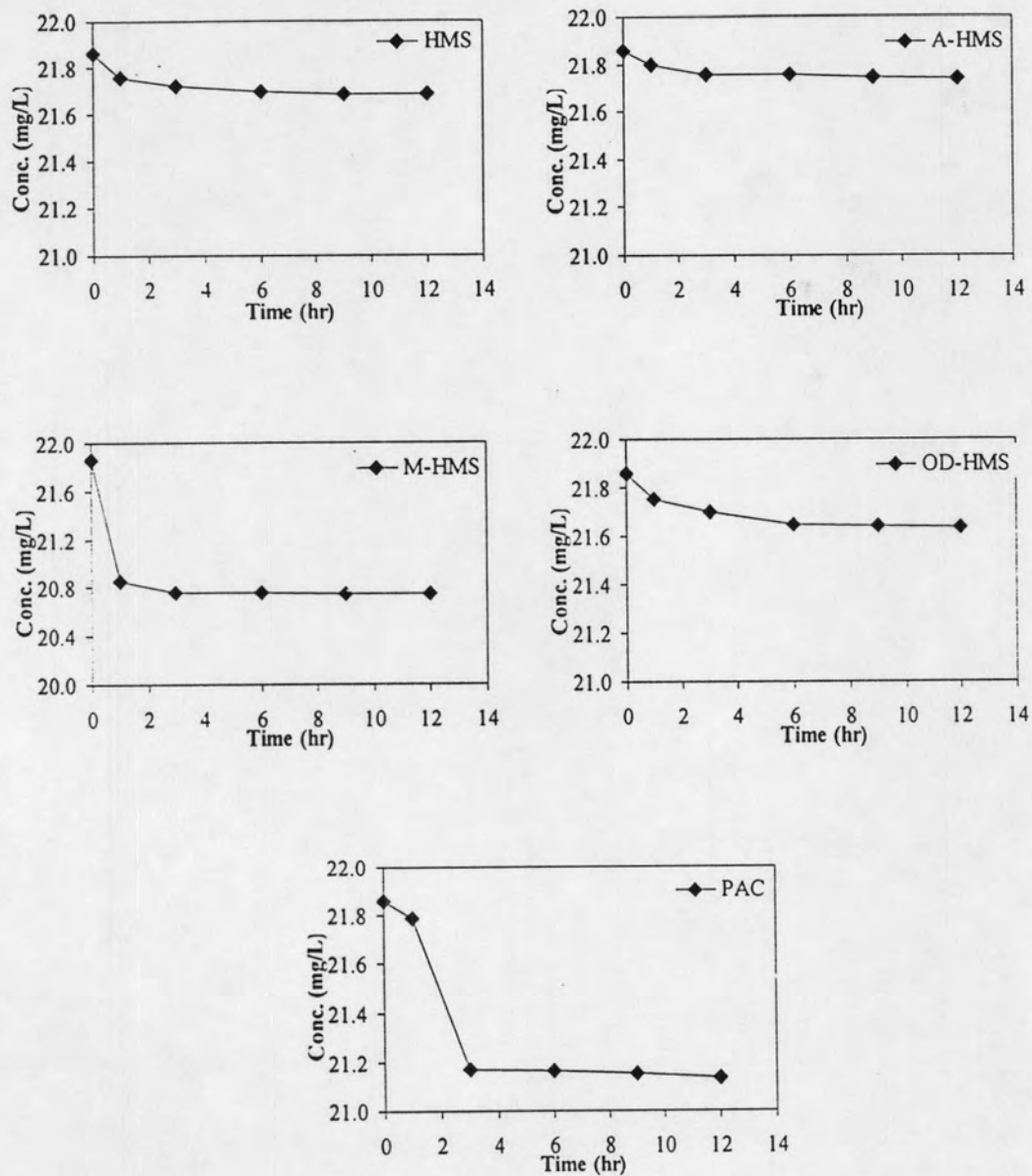
Figure 4.8 Adsorption kinetic of Cd(II) adsorption onto HMS,

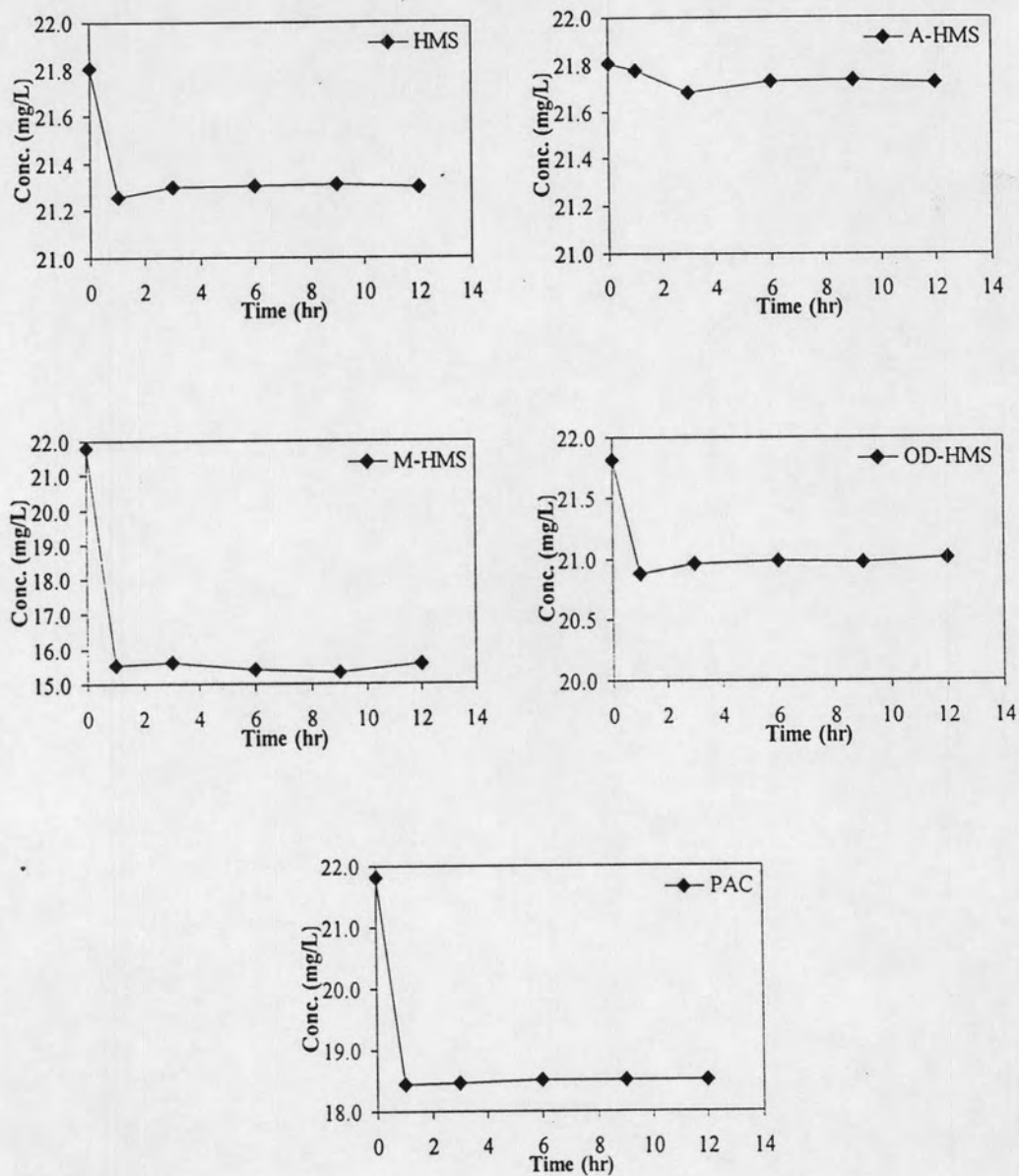functionalized HMSs, and PAC at pH 5, Ionic Strength 0.1M, Temperature 25°C

Figure 4.9 Adsorption kinetic of Cu(II) adsorption onto HMS,

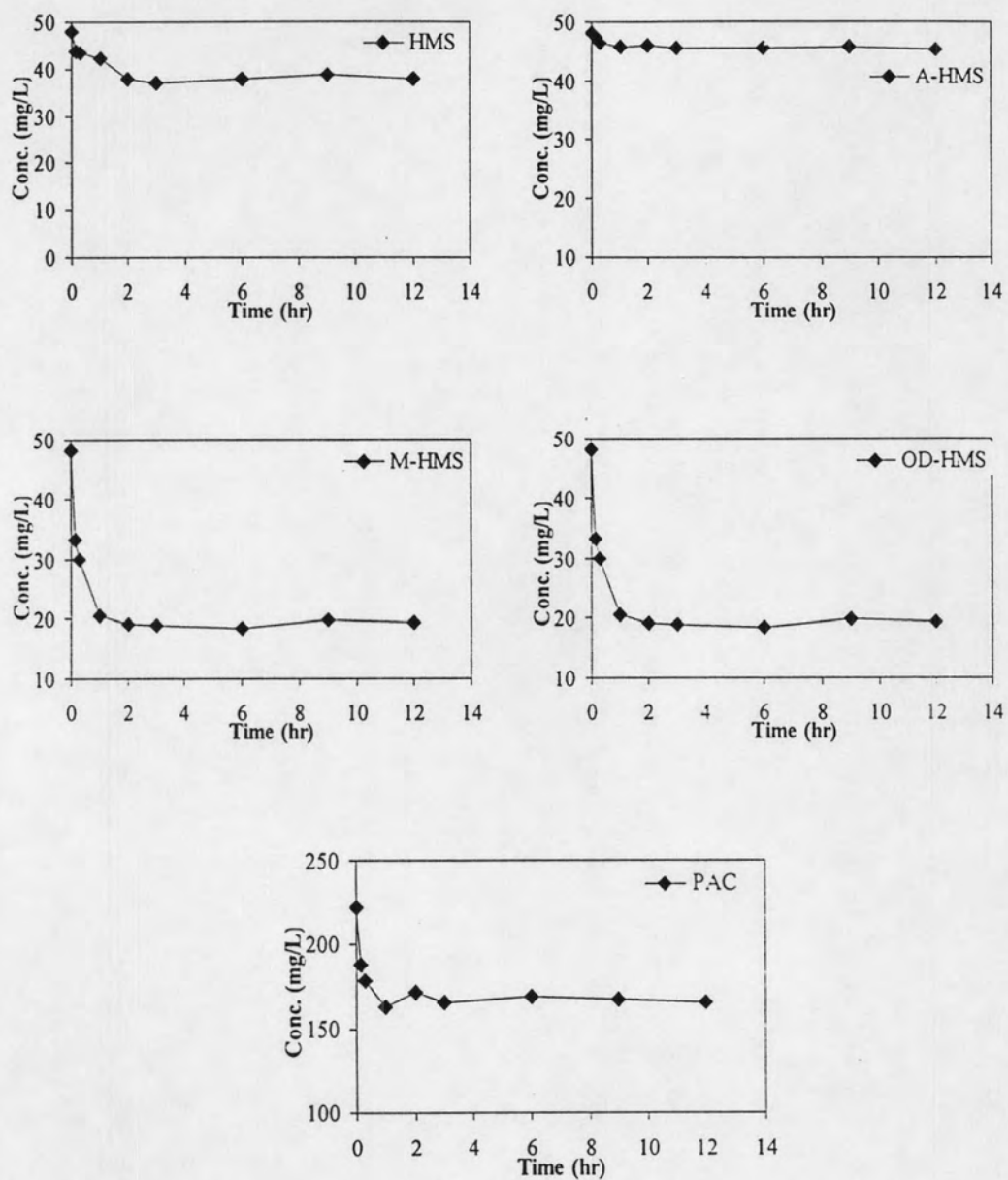functionalized HMSs, and PAC at pH 5, Ionic Strength 0.1M, Temperature 25°C

Figure 4.10 Adsorption kinetic of methylene blue adsorption onto HMS, functionalized HMSs, and PAC at pH 5, Ionic Strength 0.1M, Temperature 25°C
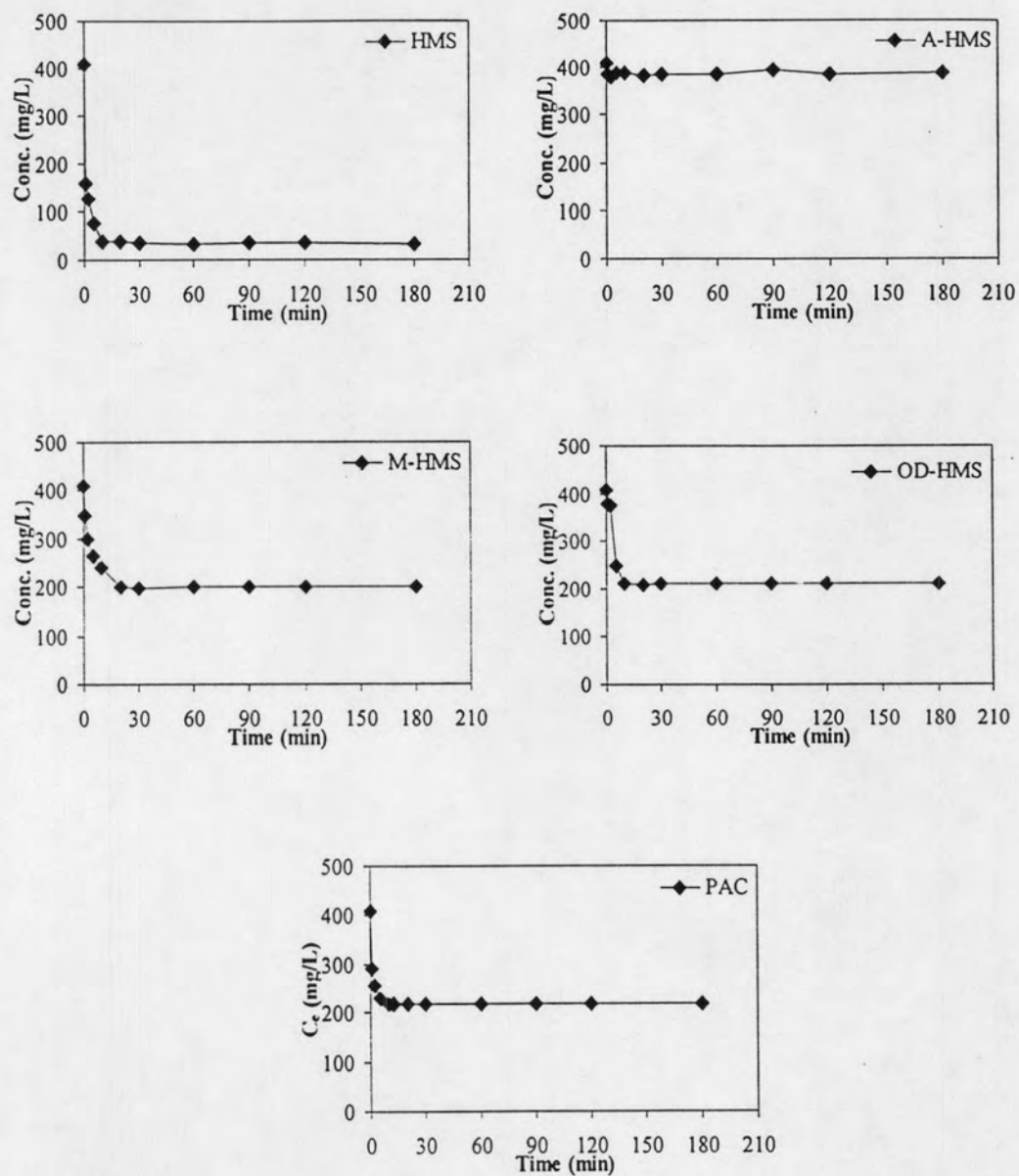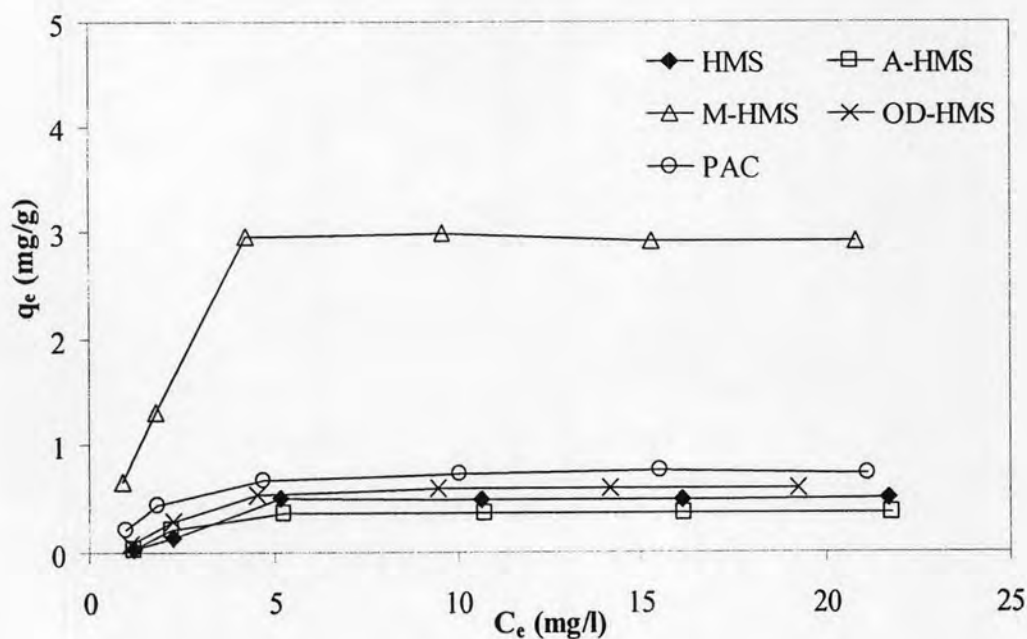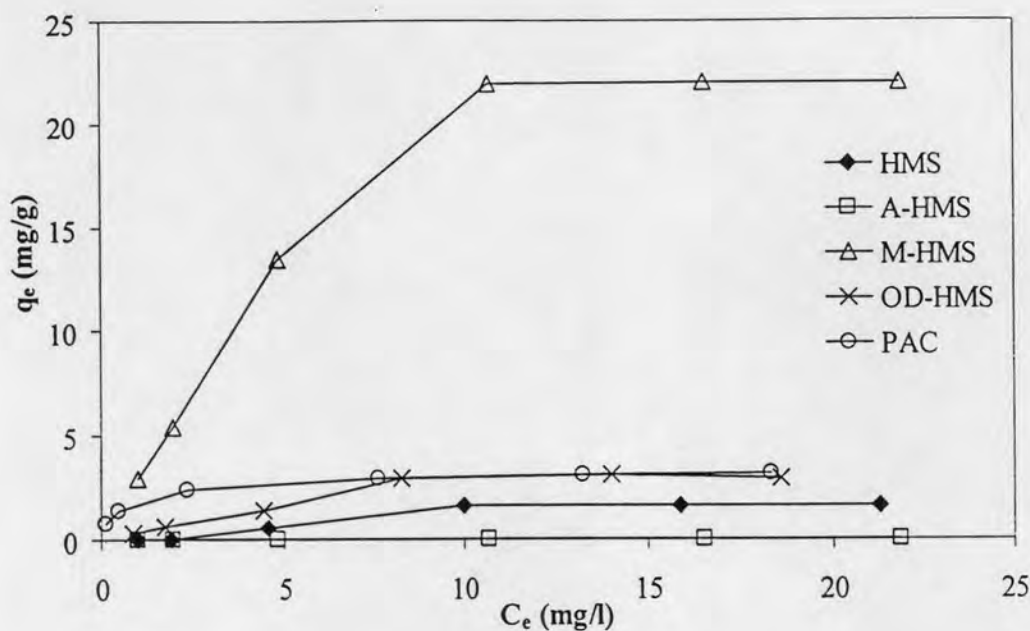
Figure 4.11 Adsorption kinetic of TX-100 adsorption onto HMS,
functionalized HMSs, and PAC at pH 5, Ionic Strength 0.1M, Temperature 25˚C

4.3 Adsorption Isotherms

In this study, adsorption mechanisms of Cd(II), Cu(II), methylene blue and TX-100 from aqueous solution onto HMS and functionalized HMSs were investigated. Their adsorption capacities were compared with PAC. Physical characteristics of these materials were investigated and their effects to adsorption mechanisms were discussed. We employed the information from adsorption isotherm together with a theoretical evaluation of the surface properties of adsorbents and adsorbate to elucidate adsorption capacities and mechanisms of HMS, functionalized HMSs and PAC. Moreover, the experimental results were fitted to Langmuir and Freundlich Equations.

4.3.1 Single solute adsorption isotherms

4.3.1.1 Heavy metals

Figure 4.12-4.13 showed adsorption isotherm of HMS, functionalized HMSs and PAC with Cd(II) and Cu(II). L shape isotherm was detected. The adsorption isotherms of Cd(II) and Cu(II) can be expressed by either Langmuir or Freundlich equations. In the case of the solution of bivalent metals, M^{2+} was the main component at pH < 6 since hydroxy species were at very low concentrations. Therefore, the measurements of the adsorption of metal ions were carried out at pH≈5 to avoid the effects of hydroxy species. Chemical reaction between metal ions and surface functional groups was suggested to be an important factor for adsorption of heavy metals.

Blitz *et al.*, (2005) reported that surface functionalization of high surface area silicas with Lewis bases for the coordination of metal cations is an effective means to rid aqueous solutions of these unwanted species. Maximum adsorption capacity was achieved using a mesoporous silica with relatively large pores reacted with a cross-linkable aminopropylsilane.

The order of both of Cd(II) and Cu(II) affinity shown in Figure 4.12-4.13 are M-HMS > PAC > OD-HMS > HMS > A-HMS. The maximum Cd(II) and Cu(II) adsorption capacities are about 3 and 22 mg/g, respectively. Moreover, silicate crystalline structure, pore size and surface area did not affect to adsorption

capacities of Cd(II) and Cu(II) on silicate surface significantly. From these results, it can be indicated that adsorption capacities of Cd(II) and Cu(II) on mercapto functionalized HMS (M-HMS) were highest comparing with the other. Morever, it might be concluded that adsorbed hydrophobic functionalized HMSs (OD-HMS and PAC) are greater than hydrophilic functionalized HMSs (A-HMS) at high level concentration.

Cadmium (Cd(II)) had bigger size of molecular size than Copper (Cu(II)) by comparing the atomic weight that atomic weight of Cadmium equals to 112.4 then Copper got around 63.5 which can confirm the results that showed Cu(II) had higher adsorption capacity than Cd(II).

3-mercaptopropyl-group of M-HMS was proposed to have chemical reaction with Cd(II) and Cu(II) that confirmed by the studies of Feng *et al.*, 1997; Lee *et al.*, 2000; Lebeau *et al.*, 2005.

Figure 4.12 Adsorption capacities of Cd(II) adsorption onto HMS, functionalized HMSs and PAC at pH 5, Ionic strength 0.1 M, Temperature 25°C
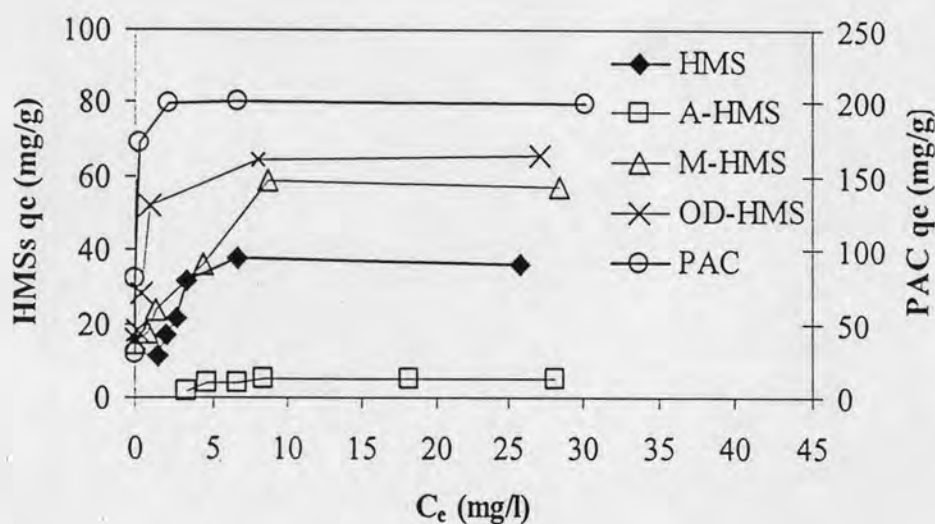
Figure 4.13 Adsorption capacities of Cu(II) adsorption onto HMS,
functionalized HMSs and PAC at pH 5, Ionic strength 0.1 M, Temperature 25°C

4.3.1.2 Methylene blue

Figure 4.14 shows methylene blue (MB) adsorption isotherms of
HMS, functionalized HMSs and PAC. L shape isotherm was detected, which are
consistent with other research works (Janos *et al.*, 2003; Espantaleon *et al.*, 2003;
Mohamed *et al.*, 2003). The adsorption isotherms of MB can be expressed by either
Langmuir or Freundlich equations. Van der Waals interaction was suggested to be an
important factor for adsorption of ionic dyes. The order of this affinity shown in
Figure 4.14 is PAC > OD-HMS > M-HMS > HMS > A-HMS.

This order, except for PAC, is in agreement with the surface
charge of HMSs. OD-HMS, HMS and M-HMS have neutral surface charge in pH 5,
but A-HMS had positive surface charge, which explained the lowest adsorption of
MB. Although it was reported that hydrogen bonding is the major attractive force for
MB, hydrogen bonding between amino-group of A-HMS and MB did not increase the
adsorption capacity of MB than any HMSs. For M-HMS and HMS, that had the
similar surface charge but hydrophobic surface (M-HMS) had greater than
hydrophilic surface (HMS) that meant the electrostatic interaction still important in

MB adsorption. PAC had a higher surface area than any HMSs, and the surface of PAC was highly heterogeneous with different organic groups. The ionic dyes can access to the micro pores of PAC. It was estimated that these factors overcome the positive surface charge of PAC, and gave it a highest adsorption capacity for MB. It was reported that at pH 4-6 surface charge of the surface didn't effect to adsorption capacity of ionic dyes significantly (Al-Ghouti *et al.*, 2003; Mohamed, 2003), which may be caused by the surface charges of HMSs do not significantly change in this pH range.

MB is cationic dye that suggested having high affinity to anionic surface. However, van der Waals force between hydrophobic surfaces (M-HMS and PAC) and MB molecule can enhance adsorption of MB, as well as the formation of hydrogen bonds between hydroxyl group (HMS) and amino group (A-HMS) on hydrophilic surface can a little bit increase the adsorption capacity. In case of OD-HMS, combined effect of van der Waals force without repulsive electrostatic force caused the highest MB adsorption capacity. Since HMS, had nearly neutral charge at pH 4-7, effect of electric charge can be neglected, hence adsorption capacities of HMS for MB were not high compared with OD-HMS. A-HMS, which had strong positive charge, had low adsorption capacity for MB because of competition between repulsion force of charges and hydrogen bonding (A-HMS).
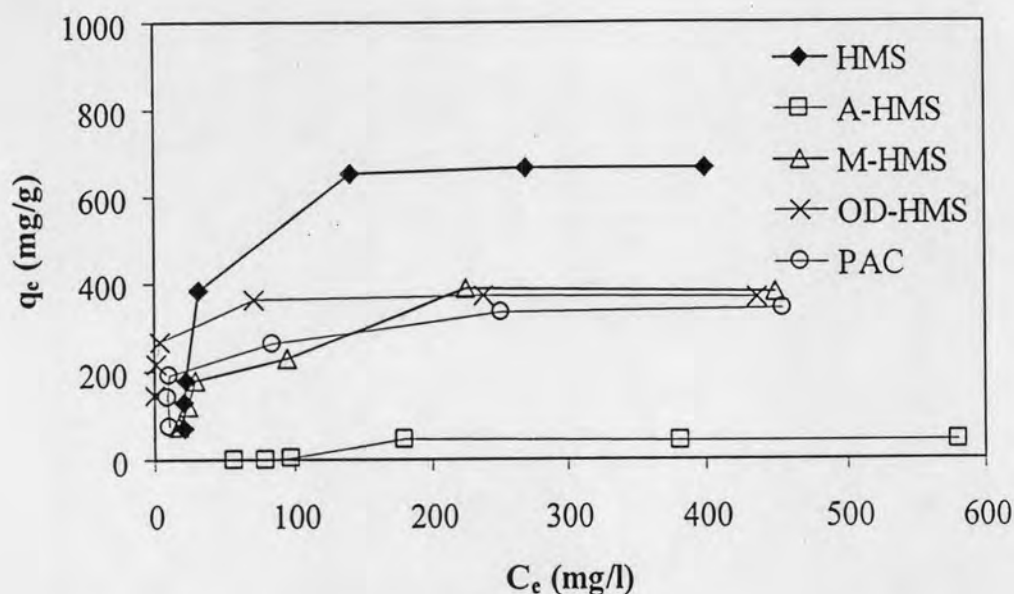

Figure 4.14 Adsorption capacities of methylene blue adsorption onto HMS, functionalized HMSs and PAC at pH 5, Ionic strength 0.1 M, Temperature 25˚C.

4.3.1.3 TX-100

Figure 4.15 presents adsorption isotherms of TX-100 on HMS, functionalized HMSs and PAC. Langmuir and Freundlich equations were applied to each isotherm. It is clear that pristine HMS has the highest adsorption capacity (about 620 mg/g) compared with functionalized HMSs and PAC (around 370 mg/g, except A-HMS). Hydrophobic modified HMSs (M-HMS and OD-HMS) had higher adsorption capacity (about 390 and 380 mg/g, respectively) than amino functionalized HMS (A-HMS). Table 4.10 shows the Langmuir and Freundlich equation parameters of TX-100 adsorption on HMS, functionalized HMSs and PAC. Linear regression of HMSs and PAC adsorption data using Langmuir Isotherm shows better correlation than regression using Freundlich isotherm. But A-HMS not only had the lowest adsorption capacity but also shows sigmoidal pattern of TX-100 adsorption, which is different from other HMSs.

Obviously, TX-100 was adsorbed onto solid surface of hydrophilic adsorbents (HMS) by hydrogen bonding between ethoxylate chain and silanol groups. On the other hand, hydrophobic adsorbents (M-HMS, OD-HMS and PAC) adsorbed TX-100 mainly by van der Waals force between adsorbent surfaces and alkylchain of TX-100. TX-100 was adsorbed on A-HMS, a hydrophilic adsorbent, by hydrogen bonding between grafted amino functional groups on the surface and ethoxylate chain of TX-100. However, self-aggregation of TX-100 molecules can occur at a higher concentration, than the critical micelle concentration (cmc) of 143 mg/l. Aggregation phenomena of TX-100 on hydrophilic and hydrophobic surfaces are different, and also affect adsorption isotherm. For hydrophobic adsorbent, molecule of TX-100 interacts with solid surface and laterally with hydrophobic chain of the molecules that already adsorbed (a half micelle size). For hydrophilic adsorbent, hydrophobic chain (alkyl chain) of adsorbed molecule can create active hydrophobic adsorption sites. This causes the adsorption of further layer (bilayer) and/or surface aggregation that have a similar surface-aggregation number as the cmc aggregation number in solution (Clunie et al., 1983). Complete aggregation on the surface of the hydrophilic adsorbents cause higher adsorption capacity than half-micelle-size aggregation of hydrophobic adsorbents.

Figure 4.15 Adsorption capacities of TX-100 adsorption onto HMS, functionalized HMSs and PAC at pH 5, Ionic strength 0.1 M, Temperature 25°C.

4.3.2 Effect of pH

To reveal the effects of pH on the adsorption capacities of HMS, functionalized HMSs and PAC were investigated by varying pH of solution from 3-5 for Cd(II) and Cu(II) and varying pH of solution from 5-9 for methylene blue and TX-100 controlled by phosphate buffer.

Theoretically, increase of negative charge on surface by increasing of pH could enhance adsorption capacity of Cd(II), Cu(II) and methylene blue. But in TX-100, its adsorption capacity is good when decreasing pH. From obtained results, it was found that at pH 5 adsorption capacities of Cd(II) and Cu(II) adsorbed onto HMS, functionalized HMSs and PAC were highest, following with pH 3 for all of adsorbents. Moreover, they had a little bit different in M-HMS adsorption of Cd(II) and Cu(II).

The effect of pH on the adsorption capacity of Cd(II) and Cu(II) by HMS, functionalized HMSs and PAC were evaluated within the pH range of 3 and 5. The highest adsorption amount of Cd(II) and Cu(II) with all of adsorbents was obtained at pH 5 that showed in Figure 4.16-4.17.

The acidity of the medium can affect the metal ions uptake amount of the adsorbents because hydrogen ions in the solution could compete with Cd(II) and Cu(II) for active sites on the adsorbents surface. The possible sites on adsorbents for specific adsorption include –OH and grafted functional groups. These functional groups are dissociated at various pH values and consequently take part in surface exchange of Cd(II) and Cu(II).

The surfaces of the adsorbents are expected to be negatively charged which facilitate the adsorption of the positively charged Cd(II) and Cu(II). The increase of the pH value favors the surface of the adsorbents become negative and the adsorption capacity of Cd(II) and Cu(II) increase. Moreover, effect of positive hydronium ion at low pH on active site or functional group might cause the decrease of positive Cd(II) and Cu(II) adsorption capacities.

For TX-100, at high pH (pH 9) adsorption capacity of HMS was decreased. Actually high pH likely to be a determining parameter, because at higher pH above 7 surface charge of adsorbent changes drastically due to dissociated silanols. The adsorption of TX-100 on HMS decreases as the pH increases and this has been ascribed to change of surface charge of adsorbents. With increase in pH above the pH_{ZPC} (around 4-6.5 for HMS) the silanol sites on the adsorbents surface are progressively changed onto silicate anions (Si-O⁻). On the assumption that the TX-100 is adsorbed through hydrogen bonding between polyethoxylate chain and silanol groups on the surfaces, this can then explain the reduced adsorption with increased pH. Decreasing of adsorption capacities of APnEOs on amorphous silicate materials caused by drastic changing to negative surface by increasing pH above pH_{ZPC} was also reported by Denoyel *et al.* (1990).

For A-HMS, adsorption capacities change a little bit, same as in M-HMS. However, in OD-HMS and PAC adsorption capacities still the same in the range of pH.

Figure 4.18 showed adsorption capacities of methylene blue at different pH. methylene blue is a cationic dye, which exists in aqueous solution in form of positively charged ions. As a charged species, the degree of its adsorption onto the adsorbent surface is primarily influenced by the surface charge on the

adsorbent, which in turn is influenced by the solution pH. The removal of methylene blue by all of adsorbents increased with pH change of dye solution from 5 to 9.

With increasing pH values the adsorption rate of methylene blue on all of adsorbents tends to increase, which can be explained by the electrostatic interaction of cationic methylene blue species with the negatively charged of adsorbents surface. The electrostatic attraction force of the dye compound with the adsorbents surface is likely to be raised when the pH increases. These results had similar trends were reported in the literature for the adsorption of methylene blue onto treated activated carbon (Yamin Yasin, 2007; Almeida *et al.*, 2009; Dougan, 2009).

The results from calculated the isotherm model compared with Langmuir and Fruendlich model that showed in table 4.7-4.10 for all of adsorbents at different pH. Almost of the results showed that Langmuir isotherm model had higher correlation than Freundlich model by compared the R^2 of both isotherm models. From the obtained results, it can be suggested the adsorption phenomena onto the adsorbents was monolayer adsorption.
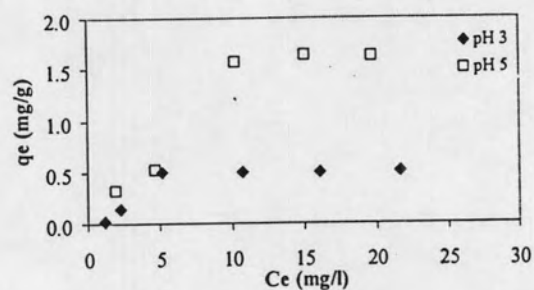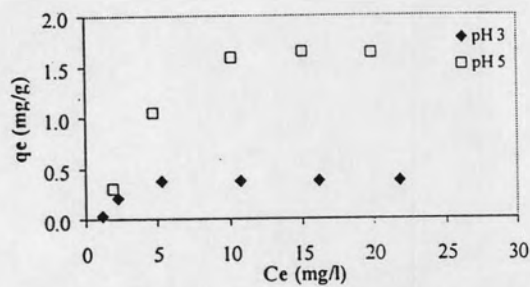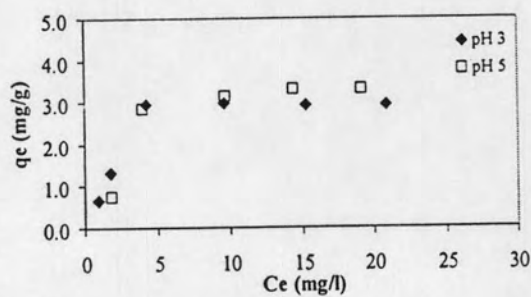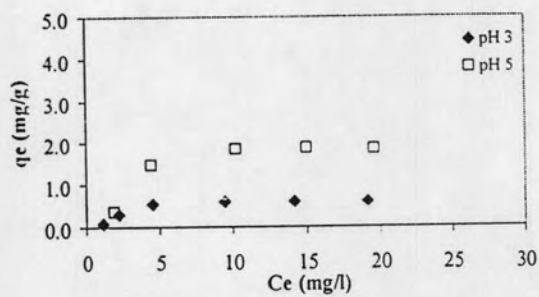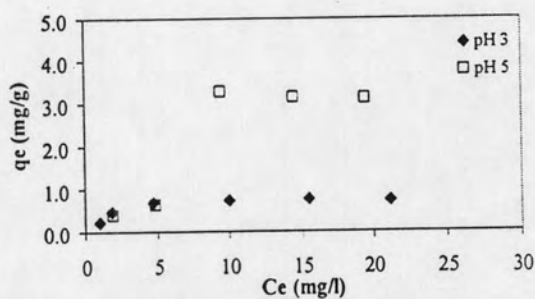
Figure 4.16 Adsorption capacities of Cd(II) adsorption on
(a) HMS, (b) A-HMS, (c) M-HMS, (d) OD-HMS and (e) PAC
at different pH, Ionic strength 0.1 M and Temperature 25 °C
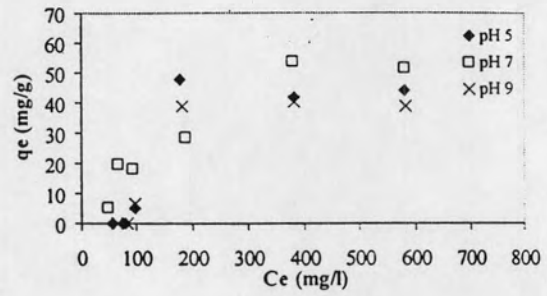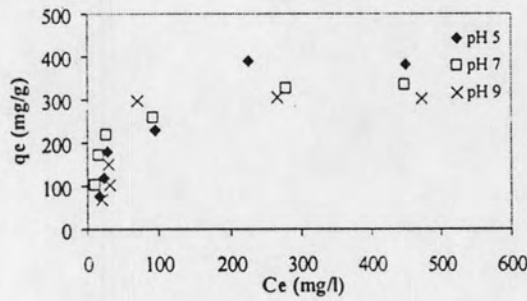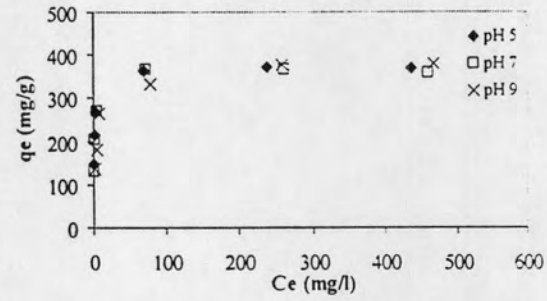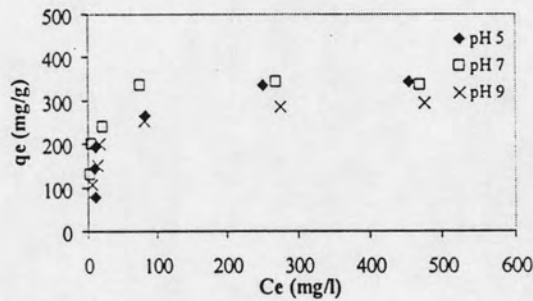
(a) HMS

(b) A-HMS
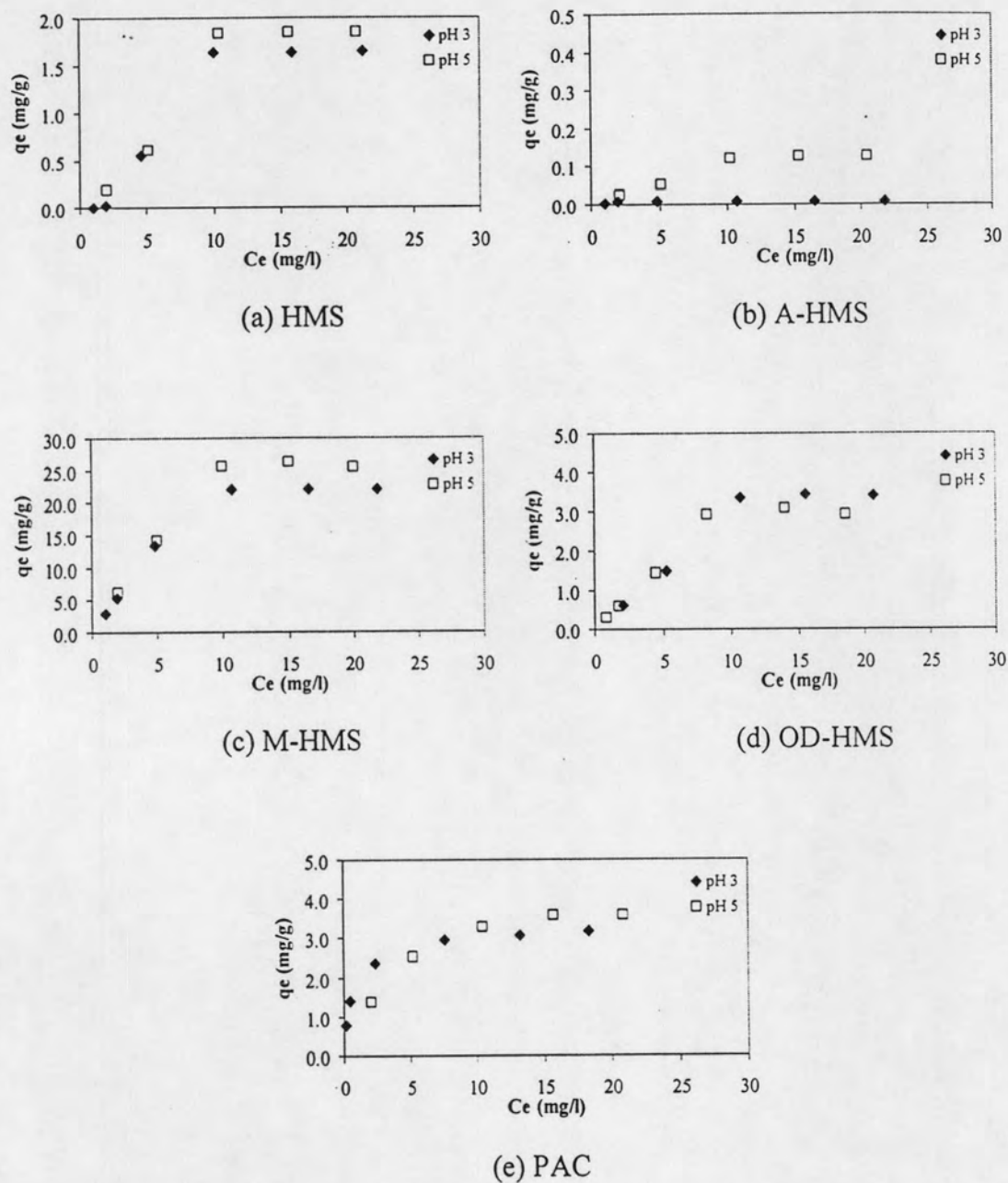
(c) M-HMS

(d) OD-HMS

(e) PAC

Figure 4.17 Adsorption capacities of Cu(II) adsorption on
(a) HMS, (b) A-HMS, (c) M-HMS, (d) OD-HMS and (e) PAC
at different pH, Ionic strength 0.1 M and Temperature 25 °C

73
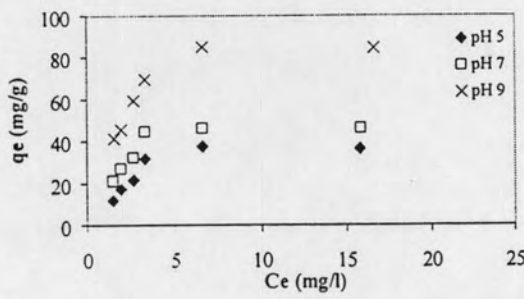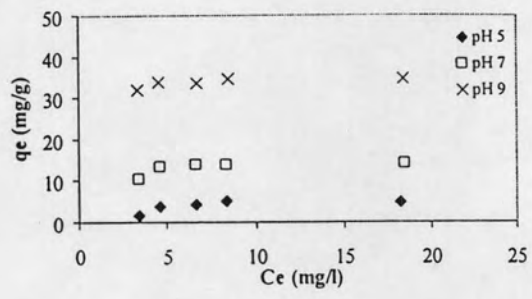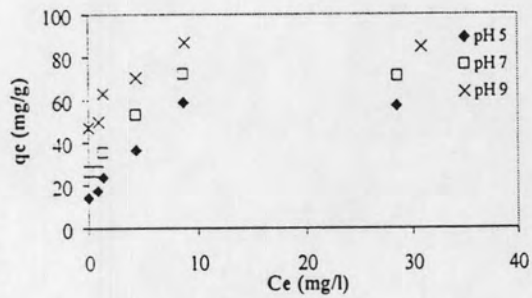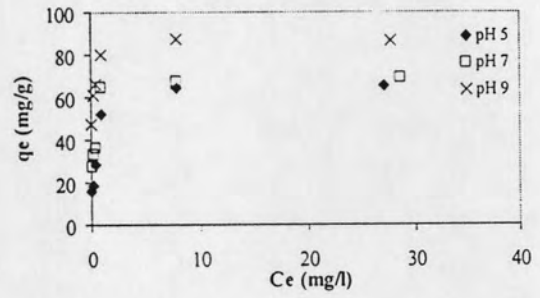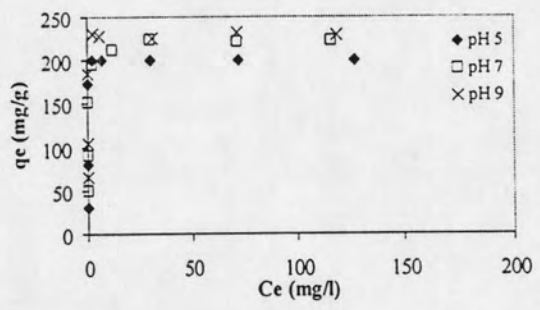
Figure 4.18 Adsorption capacities of methylene blue adsorption on

(a) HMS, (b) A-HMS, (c) M-HMS, (d) OD-HMS and (e) PAC

at different pH, Ionic strength 0.1 M and Temperature 25 °C
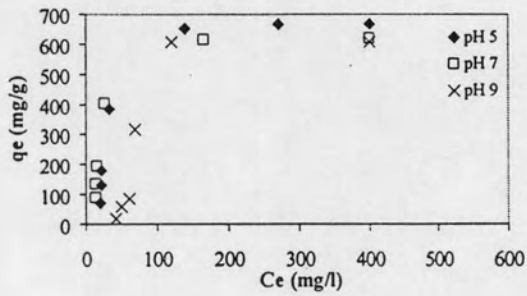
(a) HMS

(b) A-HMS

(c) M-HMS

(d) OD-HMS

(e) PAC

Figure 4.19 Adsorption capacities of TX-100 adsorption on
(a) HMS, (b) A-HMS, (c) M-HMS, (d) OD-HMS and (e) PAC
at different pH, Ionic strength 0.1 M and Temperature 25 °C

Table 4.7 Parameters of Langmuir and Freundlich isotherm model for Cd(II) adsorption on HMS, functionalized HMS and PAC at pH 3 and 5

Adsorbent	pH	Freundlich			Langmuir		
		K_f	n	R^2	S_m	b	R^2
HMS		0.2454	1.3899	0.9129	6.4725	0.0281	0.9589
A-HMS		0.2486	1.4751	0.8290	6.9252	0.0239	0.9423
M-HMS	3	0.7293	1.7062	0.7284	10.2881	1.0000	0.8816
OD-HMS		0.3344	1.5967	0.7653	6.1958	0.0347	0.9054
PAC		0.1767	0.9553	0.8611	43.8596	0.0042	0.9350
HMS		0.0431	1.0467	0.7650	-	-	0.8661
A-HMS		0.0703	1.5239	0.6819	-	-	0.8429
M-HMS	5	0.9458	2.2099	0.7848	4.8379	0.1819	0.9651
OD-HMS		0.1217	1.5487	0.7587	1.0541	0.0713	0.8992
PAC		0.2862	2.6767	0.7922	-	-	0.9398

Table 4.8 Parameters of Langmuir and Freundlich isotherm model for Cu(II) adsorption on HMS, functionalized HMS and PAC at pH 3 and 5

Adsorbent	pH	Freundlich			Langmuir		
		K_f	n	R^2	S_m	b	R^2
HMS		0.1023	1.1414	0.9600	5.8928	0.0155	0.9929
A-HMS		0.0041	0.4398	0.8871	-	-	0.9077
M-HMS	3	19.3865	5.7078	0.8243	28.0112	29.7500	0.9791
OD-HMS		20.7014	0.3844	0.9311	-	-	0.9803
PAC		399.4846	0.7599	0.9190	-	-	0.9803
HMS		0.0080	0.4974	0.9098	-	-	0.9293
A-HMS		0.0045	3.6232	0.4558	0.0134	0.2912	0.7650
M-HMS	5	3.4475	1.4620	0.9365	50.2513	0.0611	0.9950
OD-HMS		0.3907	1.2673	0.9489	9.9800	0.0363	0.9971
PAC		1.5718	3.5537	0.9557	2.8466	2.8584	0.9754

Table 4.9 Parameters of Langmuir and Freundlich isotherm model for methylene blue adsorption on HMS, functionalized HMS and PAC at pH 5, 7 and 9

Adsorbent	pH	Freundlich			Langmuir		
		K_f	n	R^2	S_m	b	R^2
HMS		12.9808	2.1673	0.7214	81.9672	0.1242	0.8940
A-HMS		1.5765	2.5056	0.4859	13.3333	0.0489	0.6643
M-HMS	5	18.6552	2.4863	0.8780	66.2252	0.3578	0.9001
OD-HMS		35.3265	4.0016	0.8664	44.6429	9.7391	0.7465
PAC		186.5091	49.7512	0.6237	200.0000	25.0000	0.9934
HMS		12.8529	2.1413	0.6764	95.2381	0.1004	0.8669
A-HMS		1.4754	2.7020	0.5245	8.9686	0.0738	0.6798
M-HMS	7	21.3354	2.6171	0.9064	38.7597	1.0000	0.8741
OD-HMS		34.9945	4.6904	0.8063	46.5116	7.9630	0.8168
PAC		165.5770	16.3399	0.8962	204.0816	9.8000	0.9620
HMS		12.3453	2.2442	0.7295	69.9301	0.1410	0.9010
A-HMS		1.8531	3.2425	0.5076	7.2202	0.1302	0.6738
M-HMS	9	22.1309	3.0760	0.9078	50.0000	0.9174	0.8940
OD-HMS		34.1901	4.8544	0.8275	40.1606	15.5625	0.6620
PAC		176.6851	24.0385	0.7909	204.0816	16.3333	0.9528

Table 4.10 Parameters of Langmuir and Freundlich isotherm model for TX-100 adsorption on HMS, functionalized HMS and PAC at pH 5, 7 and 9

Adsorbent	pH	Freundlich			Langmuir		
		K_f	n	R^2	S_m	b	R^2
HMS		23.3238	1.6504	0.7443	3333.3333	0.0017	0.6369
A-HMS		0.0019	0.5929	0.8088	-	-	0.8680
M-HMS	5	28.6352	2.2056	0.8827	526.3158	0.0115	0.9161
OD-HMS		203.5167	8.7336	0.9383	312.5000	6.4000	0.8342
PAC		69.7268	3.6271	0.7073	322.5806	0.0600	0.4875
HMS		43.7824	2.0700	0.7369	1666.6667	0.0058	0.7298
A-HMS		0.4205	1.2587	0.8182	-	-	0.7552
M-HMS	7	73.8244	3.7908	0.8367	370.3704	0.0407	0.9308
OD-HMS		187.9317	5.8754	0.9180	303.0303	0.2661	0.9604
PAC		134.5860	7.9051	0.8549	333.3333	5.0000	0.8548
HMS		0.3312	0.7331	0.6133	-	-	0.5812
A-HMS		0.0020	0.6046	0.7782	-	-	0.7615
M-HMS	9	29.1676	2.3941	0.7068	588.2353	0.0076	0.8433
OD-HMS		150.0376	6.0060	0.9113	322.5806	0.5962	0.8725
PAC		89.8876	4.7916	0.8651	294.1176	0.0988	0.9685

4.3.3 Bi solute adsorption isotherms

4.3.3.1 Heavy metals and TX-100

The adsorption isotherms in bi-solution between heavy metals and TX-100 were shown in Figure 4.20-4.29 and Figure 4.30-4.39 for Cd(II) and Cu(II), respectively. Effect of heavy metal on TX-100 adsorption capacities was conducted at the heavy metals (Cu(II) and Cd(II)) concentration from 1 to 20 mg/L and fixed concentration of TX-100 at 600 mg/L. Moreover, effect of TX-100 on heavy metals adsorption capacities was also studied by mixing solution between fixed concentration of Cd(II) and Cu(II) at 20 mg/L and vary concentration of TX-100 at 50-600 mg/L. These results showed that the adsorption capacity of heavy metals (both Cd(II) and Cu(II)) increased, compared with adsorption isotherms in Cd(II) and Cu(II) single-solute adsorption isotherms, and the adsorption capacity of TX-100 decreased for all of adsorbents. These trends also happened in the twist phase of bi-solute

adsorption isotherms. The order of the highest percentage in increasing adsorption capacities of Cd(II) was A-HMS > HMS > > OD-HMS > PAC > M-HMS, with the percent increasing equal 624.42%, 507.06%, 300.75%, 124.59% and 43.97%, respectively. Moreover, the results showed the order of Cu(II) adsorption capacities that was HMS > OD-HMS > PAC > M-HMS, with the percent increasing equal 97.71%, 74.45%, 58.12% and 15.00%, respectively. However, decreasing of TX-100 adsorption capacities on A-HMS in mixed solution of Cd(II) and Cu(II) was highest comparing with other adsorbents with 90.55% and 96.54%, respectively.

This result implies that presence of heavy metals (Cd(II) and Cu(II)) could reduce adsorption capacities of TX-100, especially for amino functional grafted HMS (A-HMS), which might be caused by chemical interaction between metal ions and surface functional groups that blocked active adsorption sites of HMSs and PAC for TX-100, including decrease of hydrogen bonding between TX-100 and the surfaces.
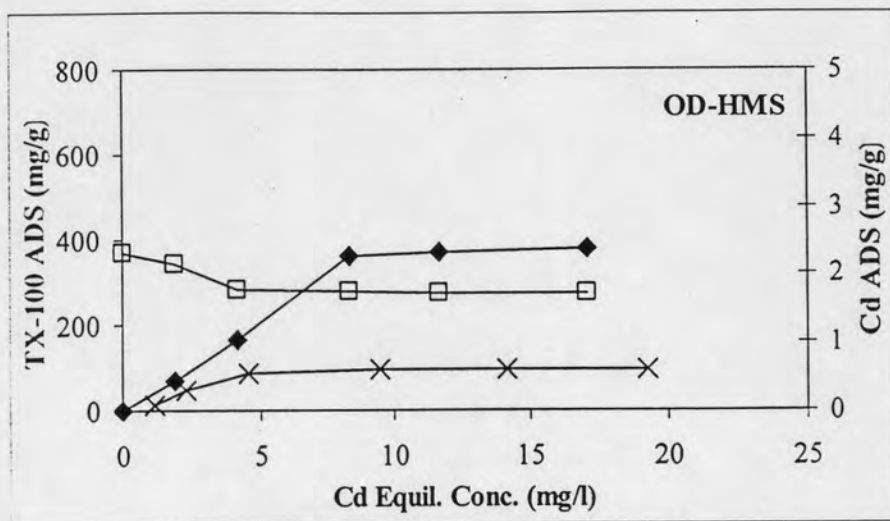
(a) Cd(II) and TX-100
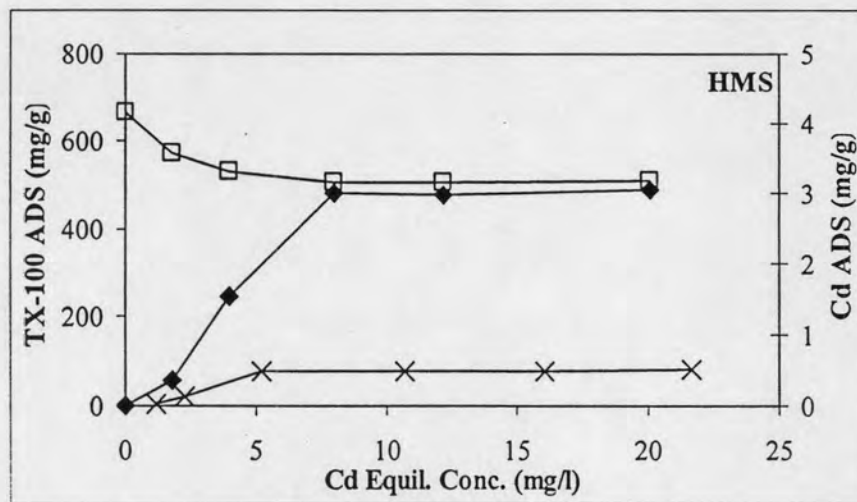
Figure 4.20 Adsorption capacity of Cd(II) on HMS by fixing initial TX-100 concentration under mixing with various Cd(II) concentration at pH 5, Ionic strength 0.1 M and Temperature 25 °C: ♦, Cd(II) Bi-solute; □, TX-100 Bi-solute; x, Cd(II) Single-solute.
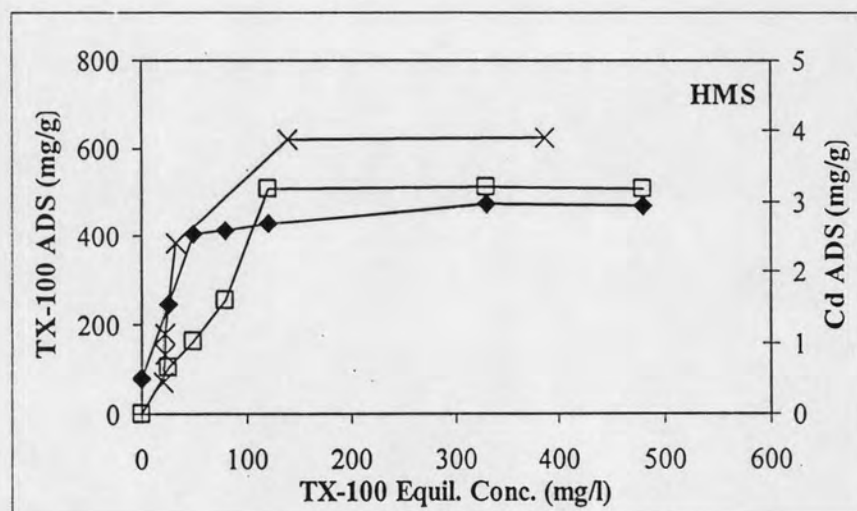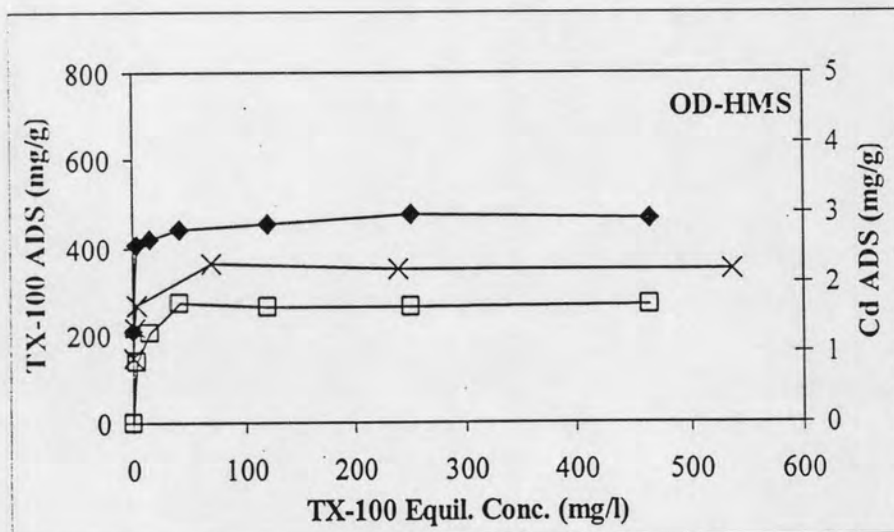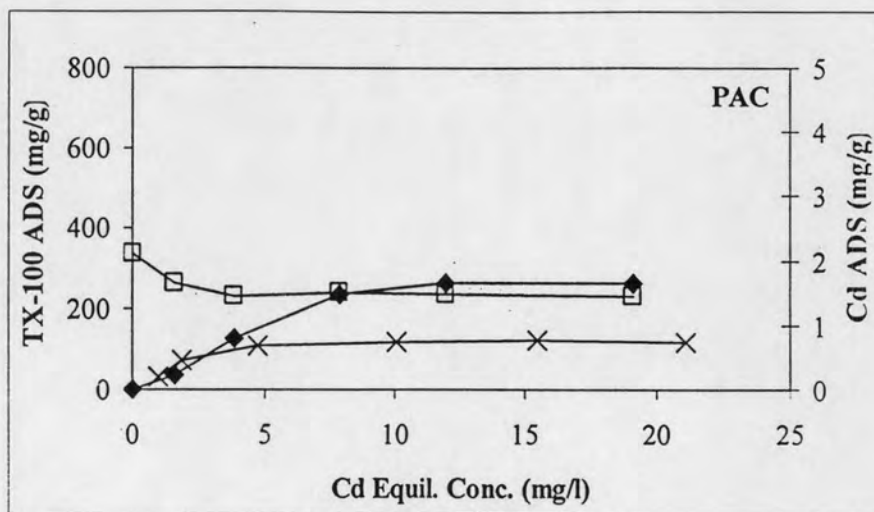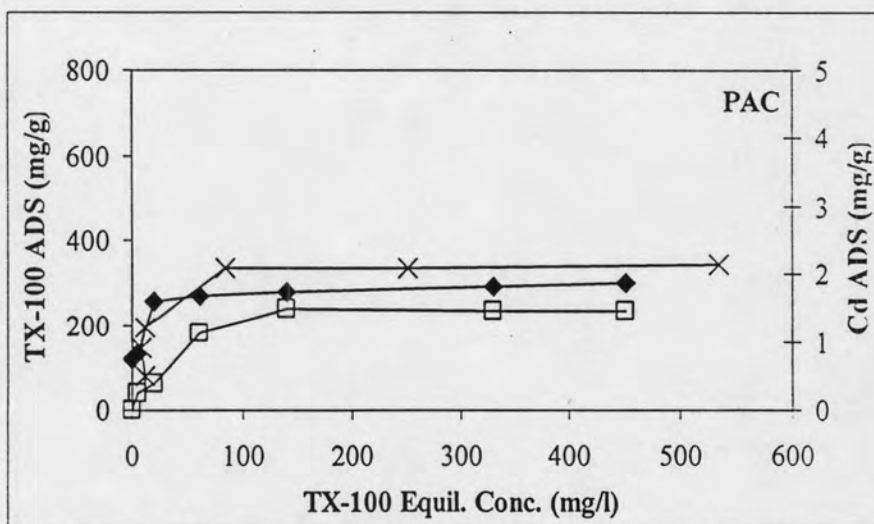

Figure 4.21 Adsorption capacity of TX-100 on HMS by fixing initial Cd(II) concentration under mixing with various TX-100 concentration at pH 5, Ionic strength 0.1 M and Temperature 25 °C: ♦, Cd(II) Bi-solute; □, TX-100 Bi-solute; x, TX-100 Single-solute.
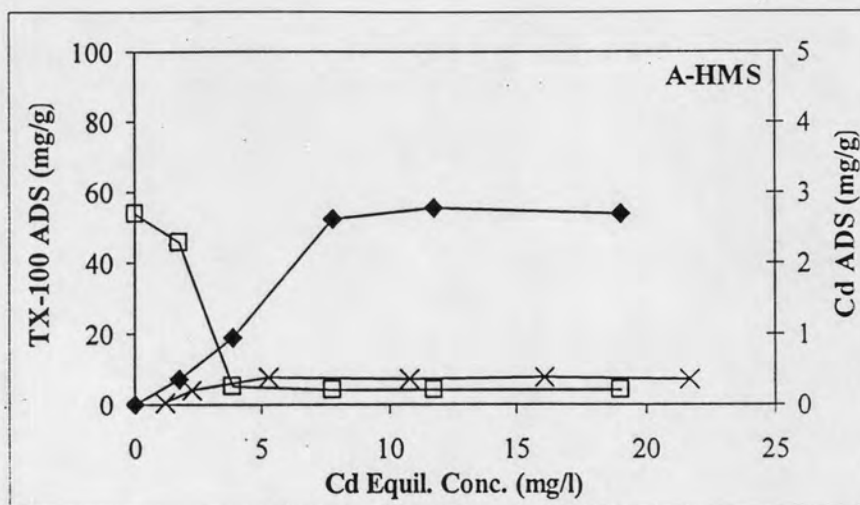
Figure 4.22 Adsorption capacity of Cd(II) on A-HMS by fixing initial TX-100 concentration under mixing with various Cd(II) concentration at pH 5, Ionic strength 0.1 M and Temperature 25 °C: ♦, Cd(II) Bi-solute; □, TX-100 Bi-solute; x, Cd(II) Single-solute.
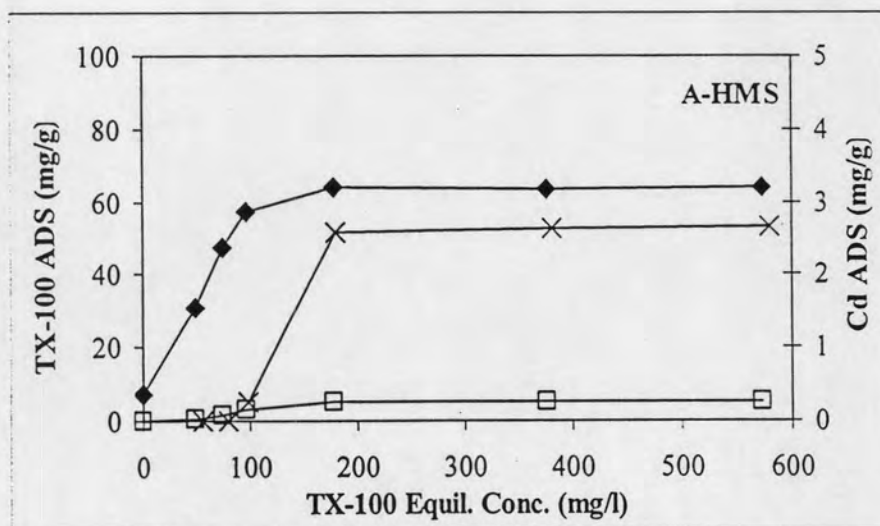
Figure 4.23 Adsorption capacity of TX-100 on A-HMS by fixing initial Cd(II) concentration under mixing with various TX-100 concentration at pH 5, Ionic strength 0.1 M and Temperature 25 °C: ♦, Cd(II) Bi-solute; □, TX-100 Bi-solute; x, TX-100 Single-solute.
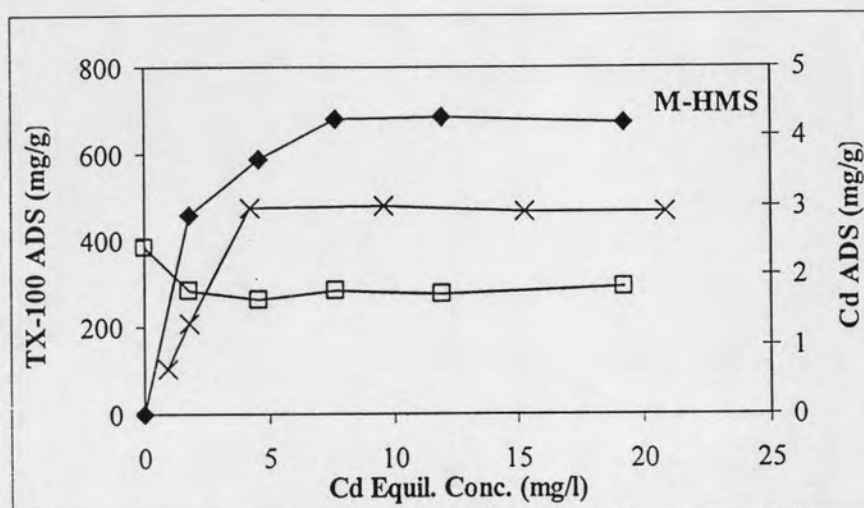
Figure 4.24 Adsorption capacity of Cd(II) on M-HMS by fixing initial TX-100 concentration under mixing with various Cd(II) concentration at pH 5, Ionic strength 0.1 M and Temperature 25 °C: ♦, Cd(II) Bi-solute; □, TX-100 Bi-solute; x, Cd(II) Single-solute.
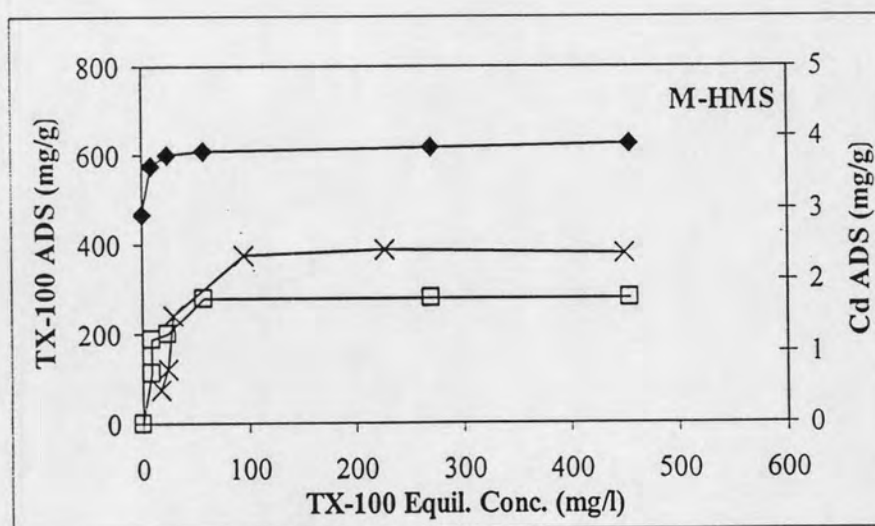
Figure 4.25 Adsorption capacity of TX-100 on M-HMS by fixing initial Cd(II) concentration under mixing with various TX-100 concentration at pH 5, Ionic strength 0.1 M and Temperature 25 °C: ♦, Cd(II) Bi-solute; □, TX-100 Bi-solute; x, TX-100 Single-solute.

Figure 4.26 Adsorption capacity of Cd(II) on OD-HMS by fixing initial TX-100 concentration under mixing with various Cd(II) concentration at pH 5, Ionic strength 0.1 M and Temperature 25 °C: ♦, Cd(II) Bi-solute; □, TX-100 Bi-solute; x, Cd(II) Single-solute.

Figure 4.27 Adsorption capacity of TX-100 on OD-HMS by fixing initial Cd(II) concentration under mixing with various TX-100 concentration at pH 5, Ionic strength 0.1 M and Temperature 25 °C: ♦, Cd(II) Bi-solute; □, TX-100 Bi-solute; x, TX-100 Single-solute.
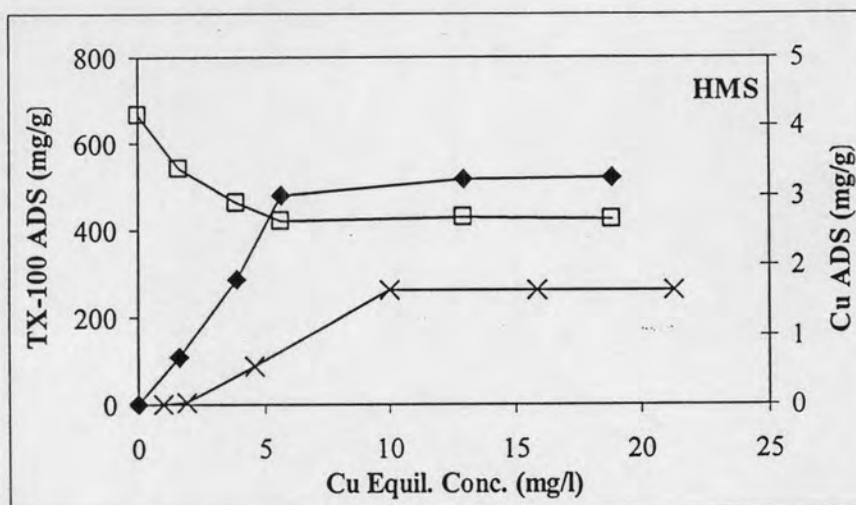
Figure 4.28 Adsorption capacity of Cd(II) on PAC by fixing initial TX-100 concentration under mixing with various Cd(II) concentration at pH 5, Ionic strength 0.1 M and Temperature 25 °C: ♦, Cd(II) Bi-solute; □, TX-100 Bi-solute; x, Cd(II) Single-solute.

Figure 4.29 Adsorption capacity of TX-100 on PAC by fixing initial Cd(II) concentration under mixing with various TX-100 concentration at pH 5, Ionic strength 0.1 M and Temperature 25 °C: ♦, Cd(II) Bi-solute; □, TX-100 Bi-solute; x, TX-100 Single-solute.

The adsorption isotherm of Cd(II) on HMS was increased, on the other hand, the adsorption isotherm showed that adsorption capacity of TX-100 on HMS decreased comparing with the single solution isotherm. The amount of Cd(II) adsorption capacities increased from 0.51 to 3.06 mg/g. These results showed and absorbed TX-100 on HMS surface might change surface characteristic of HMS, causing the bi-layer interaction of Cd(II) adsorption.

The adsorption isotherm of Cd(II) on A-HMS was increased, on the other hand, the adsorption isotherm of TX-100 on A-HMS was extremely decreased comparing with the single solution isotherm. The amount of Cd(II) adsorption capacities increased from 0.37 to 2.69 mg/g. These results showed that absorbed TX-100 on HMS surface might change surface characteristic of A-HMS, causing the bi-layer interaction of Cd(II) adsorption.

The adsorption isotherm of Cd(II) on M-HMS was increased, on the other hand, the adsorption isotherm of TX-100 on M-HMS was decreased comparing with the single solution isotherm. The amount of Cd(II) adsorption capacities increased from 2.91 to 4.19 mg/g. These results showed that absorbed TX-100 on M-HMS surface might change surface characteristics of M-HMS, causing the bi-layer interaction of Cd(II) adsorption.

The adsorption isotherm of Cd(II) on OD-HMS was increased, on the other hand, the adsorption isotherm of TX-100 on OD-HMS was decreased, comparing with the single solution adsorption. The amount of Cd(II) adsorption capacities increased from 0.59 to 2.37 mg/g. These results showed that absorbed TX-100 on OD-HMS surface might change surface characteristics of OD-HMS, causing the bi-layer interaction of Cd(II) adsorption.

The adsorption isotherm of Cd(II) on PAC was increased, on the other hand, the adsorption isotherm of TX-100 on PAC was decreased, comparing with the single solution. The amount of Cd(II) adsorption capacities were increased from 0.73 to 1.64 mg/g. These results showed that absorbed TX-100 on PAC surface might change surface characteristics of PAC, causing the bi-layer interaction of Cd(II) adsorption.

(b) Cu(II) and TX-100

Figure 4.30 Adsorption capacity of Cu(II) on HMS by fixing initial TX-100 concentration under mixing with various Cu(II) concentration at pH 5, Ionic strength 0.1 M and Temperature 25 °C: ♦, Cu(II) Bi-solute; □, TX-100 Bi-solute; x, Cu(II) Single-solute.
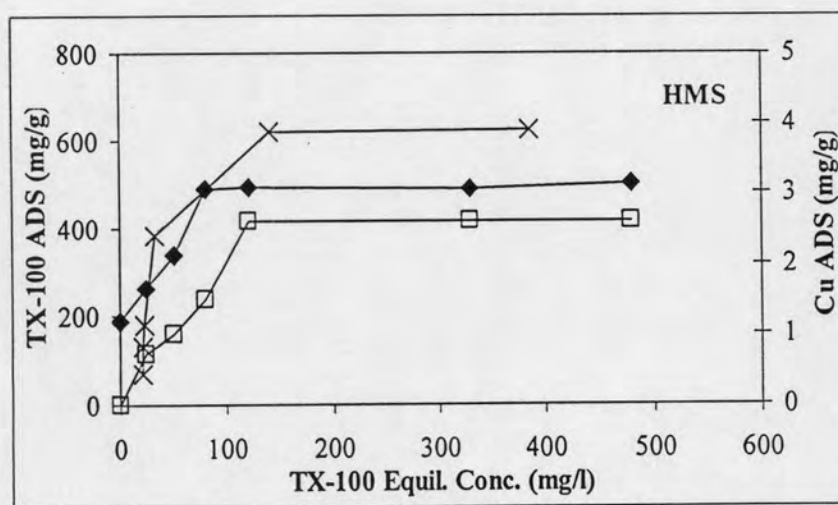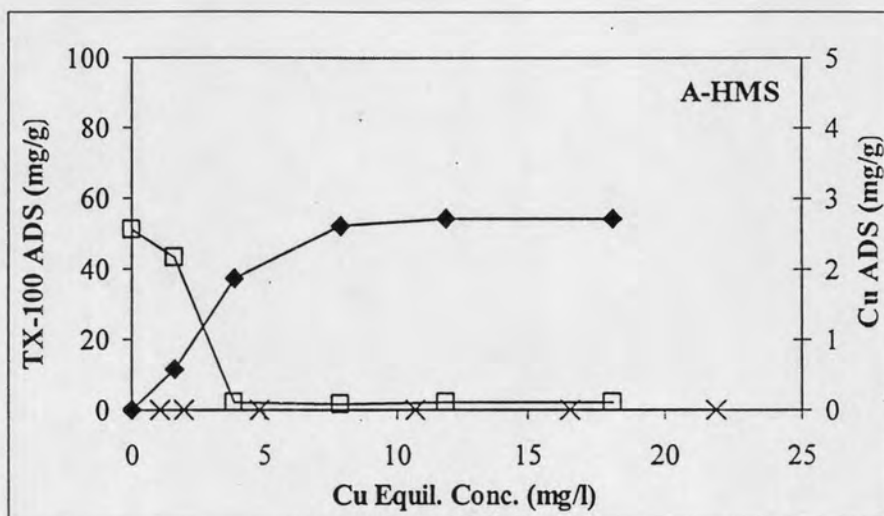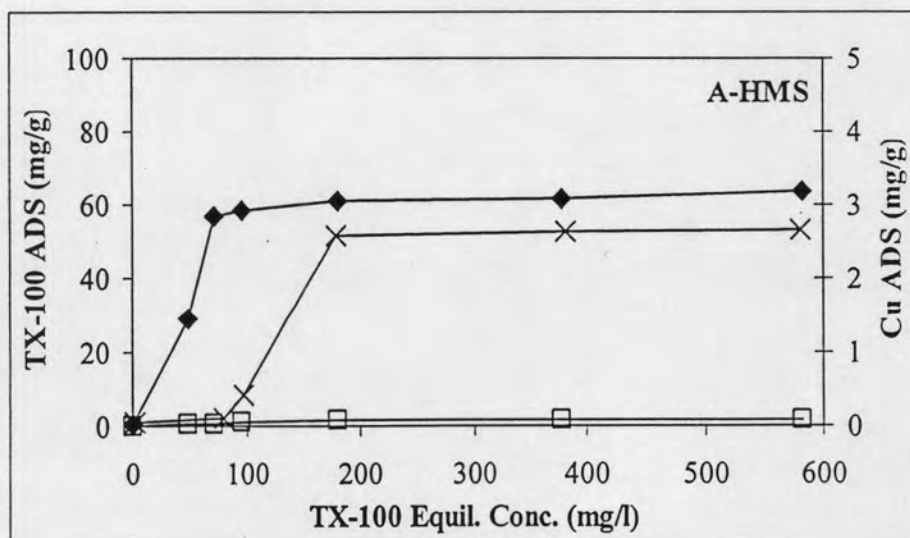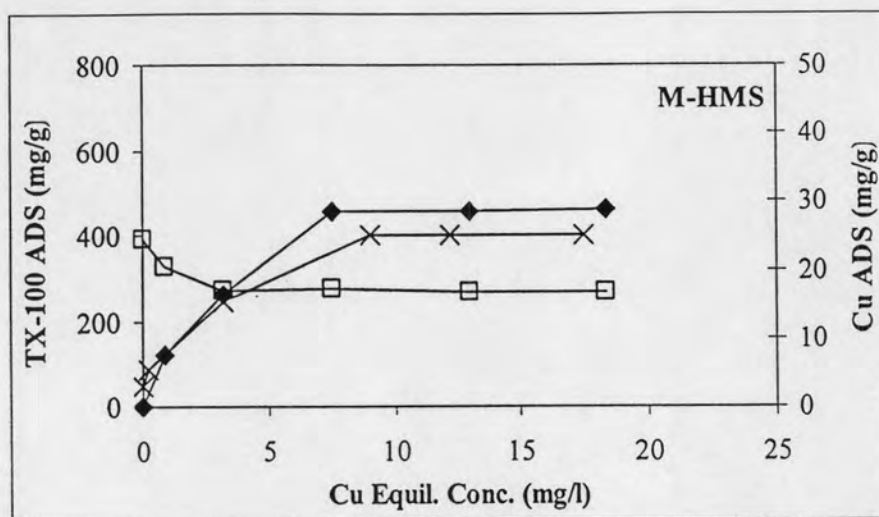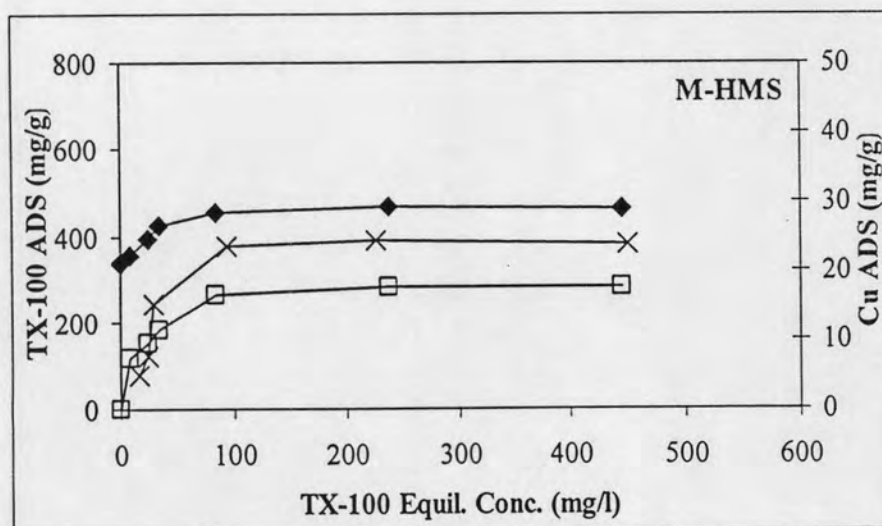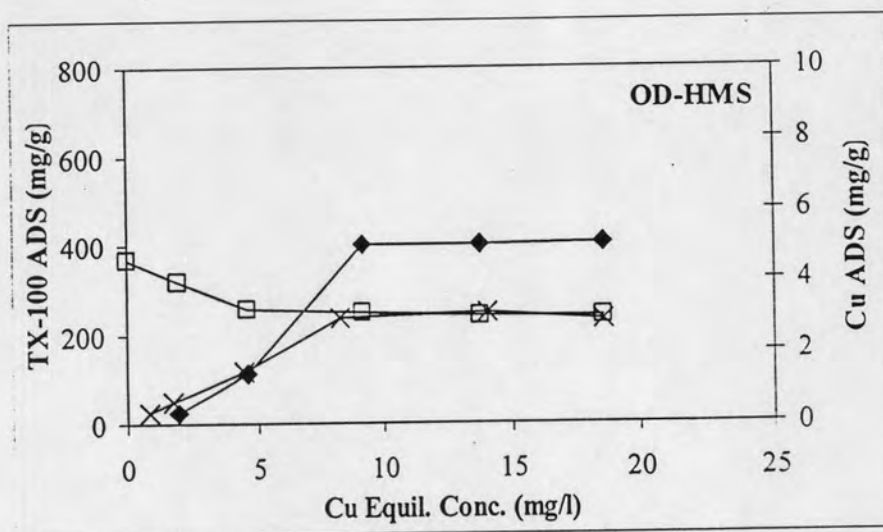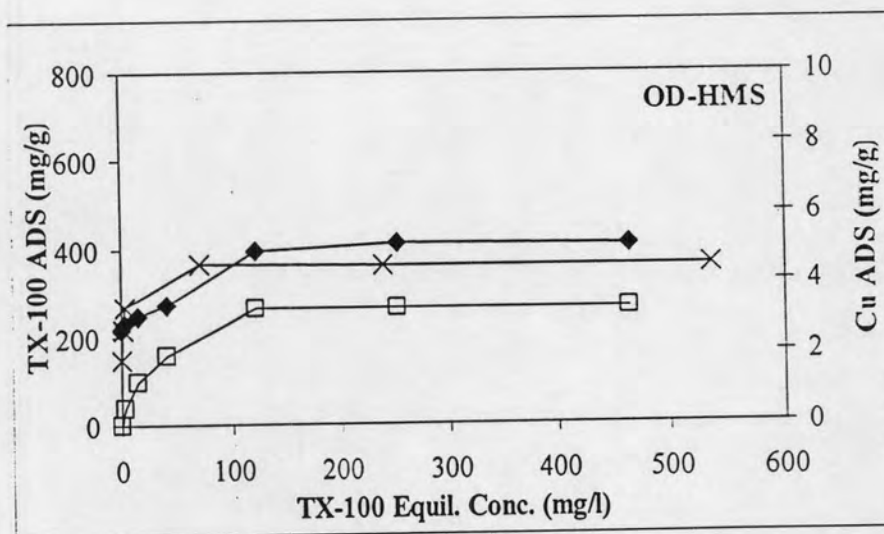

Figure 4.31 Adsorption capacity of TX-100 on HMS by fixing initial Cu(II) concentration under mixing with various TX-100 concentration at pH 5, Ionic strength 0.1 M and Temperature 25 °C: ♦, Cu(II) Bi-solute; □, TX-100 Bi-solute; x, TX-100 Single-solute.

Figure 4.32 Adsorption capacity of Cu(II) on A-HMS by fixing initial TX-100 concentration under mixing with various Cu(II) concentration at pH 5, Ionic strength 0.1 M, Temperature 25 °C: ♦, Cu(II) Bi-solute; □, TX-100 Bi-solute; x, Cu(II) Single-solute.

Figure 4.33 Adsorption capacity of TX-100 on A-HMS by fixing initial Cu(II) concentration under mixing with various TX-100 concentration at pH 5, Ionic strength 0.1 M and Temperature 25 °C: ♦, Cu(II) Bi-solute; □, TX-100 Bi-solute; x, TX-100 Single-solute.
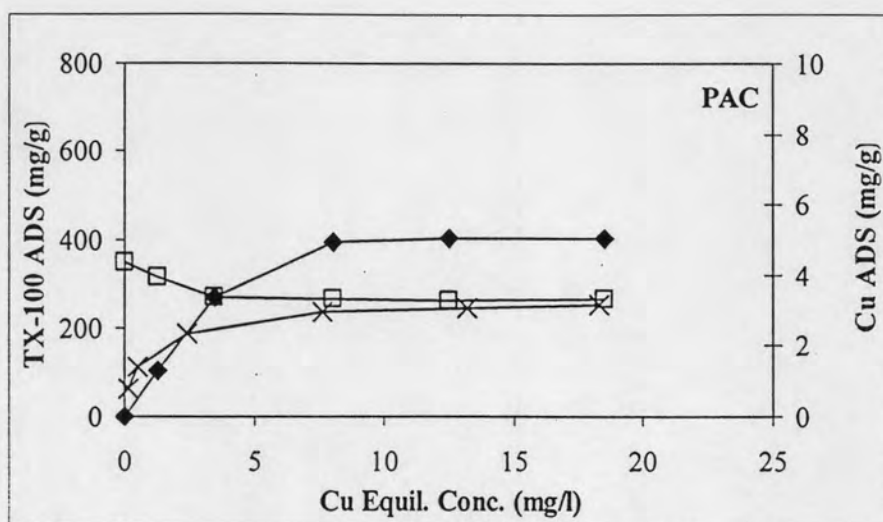
Figure 4.34 Adsorption capacity of Cu(II) on M-HMS by fixing initial TX-100 concentration under mixing with various Cu(II) concentration at pH 5, Ionic strength 0.1 M, Temperature 25 °C: ♦, Cu(II) Bi-solute; □, TX-100 Bi-solute; x, Cu(II) Single-solute.
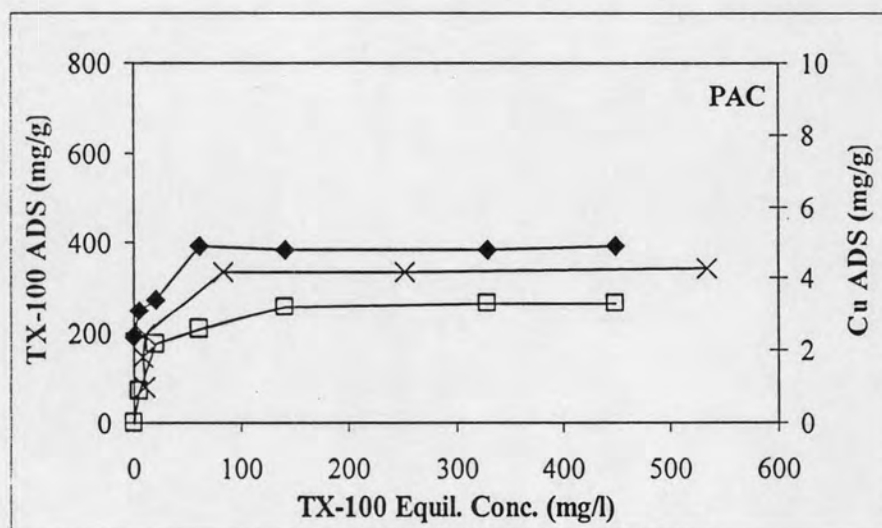

Figure 4.35 Adsorption capacity of TX-100 on M-HMS by fixing initial Cu(II) concentration under mixing with various TX-100 concentration at pH 5, Ionic strength 0.1 M and Temperature 25 °C: ♦, Cu(II) Bi-solute; □, TX-100 Bi-solute; x, TX-100 Single-solute.

Figure 4.36 Adsorption capacity of Cu(II) on OD-HMS by fixing initial TX-100 concentration under mixing with various Cu(II) concentration at pH 5, Ionic strength 0.1 M, Temperature 25 °C: ♦, Cu(II) Bi-solute; □, TX-100 Bi-solute; x, Cu(II) Single-solute.

Figure 4.37 Adsorption capacity of TX-100 on OD-HMS by fixing initial Cu(II) concentration under mixing with various TX-100 concentration at pH 5, Ionic strength 0.1 M and Temperature 25 °C: ♦, Cu(II) Bi-solute; □, TX-100 Bi-solute; x, TX-100 Single-solute.

Figure 4.38 Adsorption capacity of Cu(II) on PAC by fixing initial TX-100 concentration under mixing with various Cu(II) concentration at pH 5, Ionic strength 0.1 M, Temperature 25 °C: ♦, Cu(II) Bi-solute; □, TX-100 Bi-solute; x, Cu(II) Single-solute.

Figure 4.39 Adsorption capacity of TX-100 on PAC by fixing initial Cu(II) concentration under mixing with various TX-100 concentration at pH 5, Ionic strength 0.1 M and Temperature 25 °C: ♦, Cu(II) Bi-solute; □, TX-100 Bi-solute; x, TX-100 Single-solute.

The adsorption isotherm of Cu(II) on HMS was increased, on the other hand, the adsorption isotherm showed that adsorption capacity of TX-100 on HMS decreased comparing with the single solution isotherm. The amount of Cu(II) adsorption capacities increased from 1.65 to 3.26 mg/g. These results showed and absorbed TX-100 on HMS surface might change surface characteristic of HMS, causing the bi-layer interaction of Cu(II) adsorption.

The adsorption isotherm of Cu(II) on A-HMS was increased, on the other hand, the adsorption isotherm of TX-100 on A-HMS was extremely decreased comparing with the single solution isotherm. The amount of Cu(II) adsorption capacities increased from 0.01 to 2.70 mg/g. These results showed that absorbed TX-100 on HMS surface might change surface characteristic of A-HMS, causing the bi-layer interaction of Cu(II) adsorption.

The adsorption isotherm of Cu(II) on M-HMS was increased, on the other hand, the adsorption isotherm of TX-100 on M-HMS was decreased comparing with the single solution isotherm. The amount of Cu(II) adsorption capacities increased from 24.95 to 28.69 mg/g. These results showed that absorbed TX-100 on M-HMS surface might change surface characteristics of M-HMS, causing the bi-layer interaction of Cu(II) adsorption.

The adsorption isotherm of Cu(II) on OD-HMS was increased, on the other hand, the adsorption isotherm of TX-100 on OD-HMS was decreased, comparing with the single solution adsorption. The amount of Cu(II) adsorption capacities increased from 2.91 to 5.07 mg/g. These results showed that absorbed TX-100 on OD-HMS surface might change surface characteristics of OD-HMS, causing the bi-layer interaction of Cu(II) adsorption.

The adsorption isotherm of Cu(II) on PAC was increased, on the other hand, the adsorption isotherm of TX-100 on PAC was decreased, comparing with the single solution. The amount of Cu(II) adsorption capacities were increased from 3.17 to 5.01 mg/g. These results showed that absorbed TX-100 on PAC surface might change surface characteristics of PAC, causing the bi-layer interaction of Cu(II) adsorption.

4.3.3.2 Heavy metals and methylene blue

The adsorption isotherms in bi-solution between heavy metals and MB were shown in Figure 4.40-4.49 and Figure 4.50-4.59 for Cd(II) and Cu(II), respectively. Effects of heavy metals on MB adsorption capacities were conducted at the heavy metals (Cu(II) and Cd(II)) concentration from 1 to 20 mg/L and fixed concentration of MB at 30 mg/L, except for PAC was fixed at 100 mg/L. Moreover, effect of MB on heavy metals adsorption capacities was also studied by mixing solution between fixed concentration of Cd(II) and Cu(II) at 20 mg/L and vary concentration of MB at 5-30 mg/L and 60-150 mg/L for all HMSs and PAC respectively. These results showed that the adsorption capacity of heavy metals (both Cd(II) and Cu(II)) and MB decreased when compared with adsorption isotherms in single-solute for all of adsorbents. These changes also happened in the twist phase of bi-solute adsorption isotherms. The order of the highest change in decreasing adsorption capacities for Cd(II) is A-HMS > OD-HMS > HMS > PAC > M-HMS, with the percent decreasing at 82.20%, 55.13%, 30.64%, 29.72% and 12.95%, respectively. For Cu(II), the results showed the order that was A-HMS > M-HMS > HMS > OD-HMS > PAC, with the percent decreasing at 50.49%, 48.90%, 35.08%, 34.24% and 32.35%, respectively. However, decreasing of TX-100 adsorption capacities on A-HMS was highest for mixed with Cd(II) and HMS (52.94% and 53.02%, respectively).

Decreasing in adsorption capacities of both heavy metals and MB might caused by the effect of competition to access active surface functional groups without bi-layer adsorption. Effect of heavy metals on MB adsorption capacities of hydrophobic HMSs (M-HMS and OD-HMS) trended to be smaller than hydrophilic HMSs (HMS and A-HMS), except for PAC.

(a) Cd(II) and methylene blue
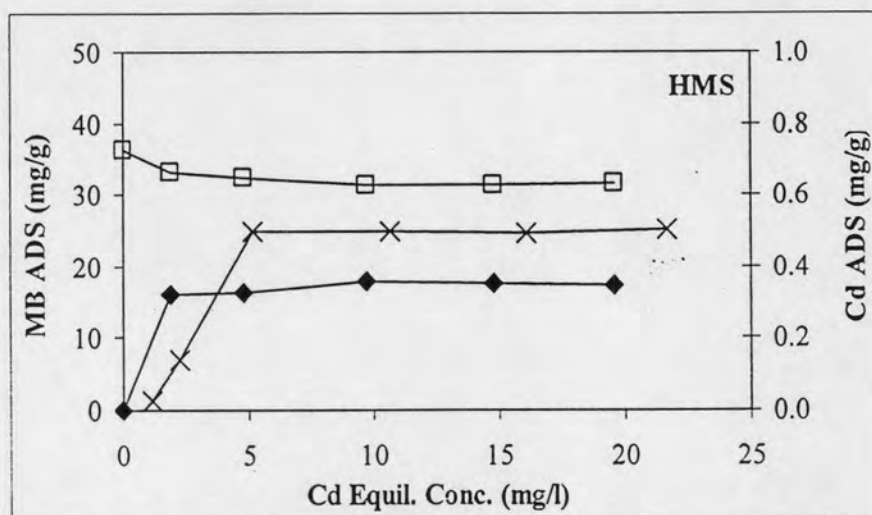
Figure 4.40 Adsorption capacity of Cd(II) on HMS by fixing initial MB concentration under mixing with various Cd(II) concentration at pH 5, Ionic strength 0.1 M, Temperature 25 °C: ♦, Cd(II) Bi-solute; □, MB Bi-solute; x, Cd(II) Single-solute.
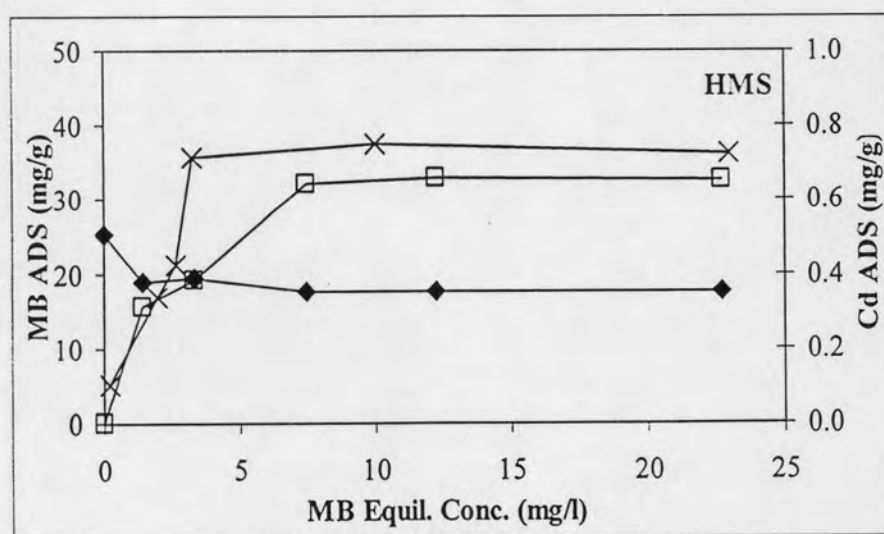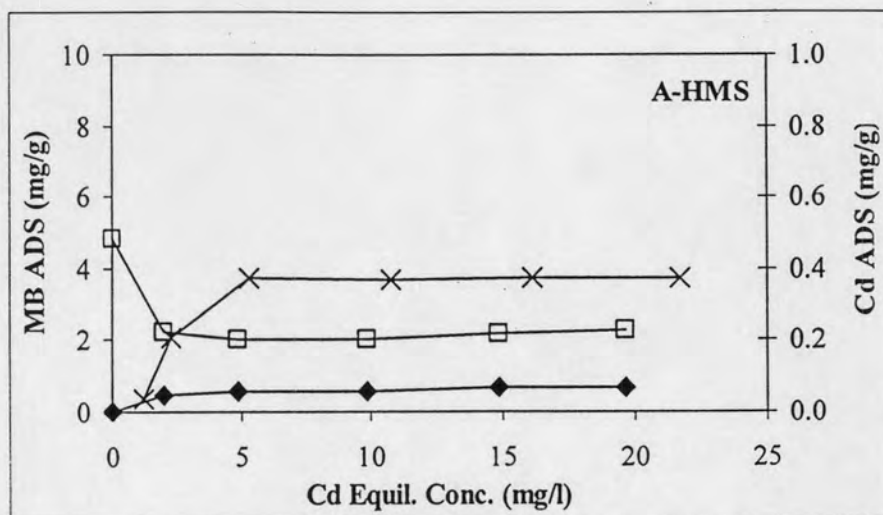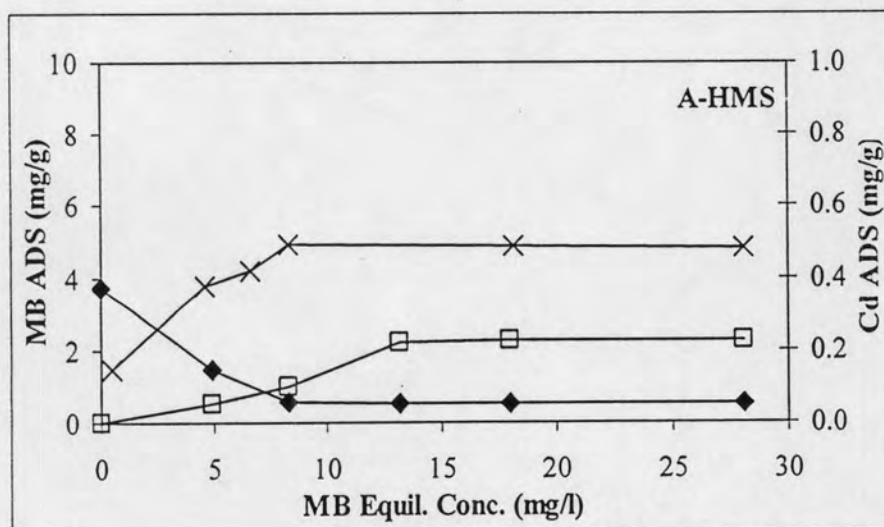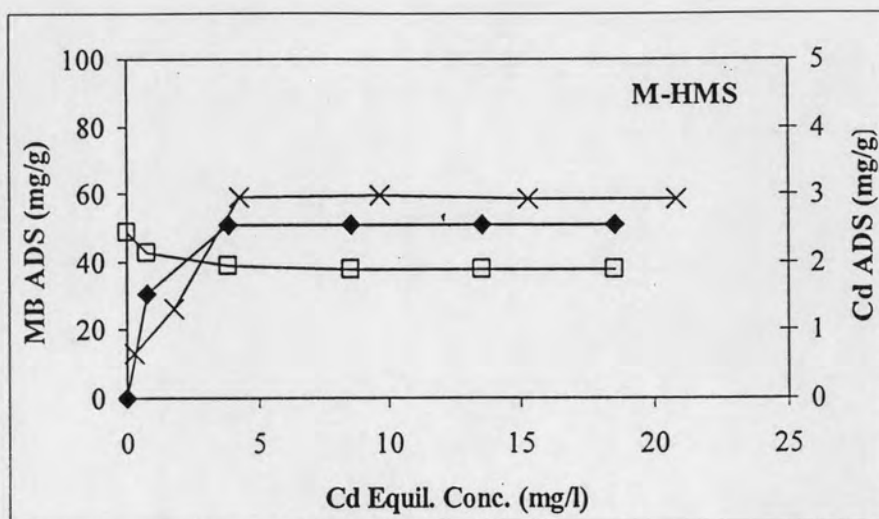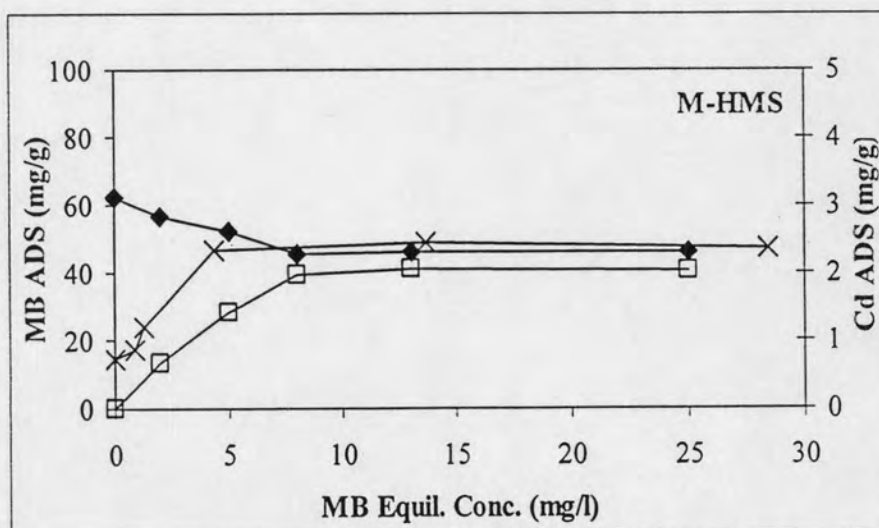

Figure 4.41 Adsorption capacity of MB on HMS by fixing initial Cd(II) concentration under mixing with various MB concentration at pH 5, Ionic strength 0.1 M and Temperature 25 °C: ♦, Cd(II) Bi-solute; □, MB Bi-solute; x, MB Single-solute.
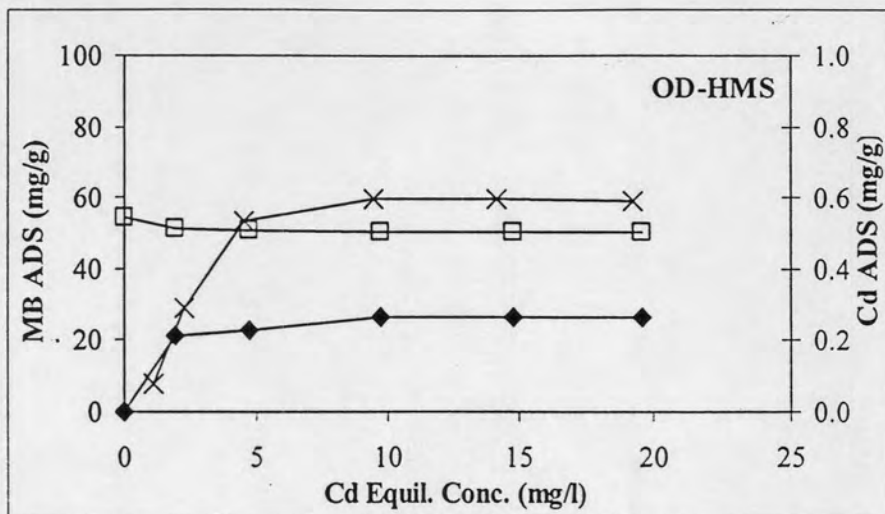
Figure 4.42 Adsorption capacity of Cd(II) on A-HMS by fixing initial MB concentration under mixing with various Cd(II) concentration at pH 5, Ionic strength 0.1 M, Temperature 25 °C: ♦, Cd(II) Bi-solute; □, MB Bi-solute; x, Cd(II) Single-solute.
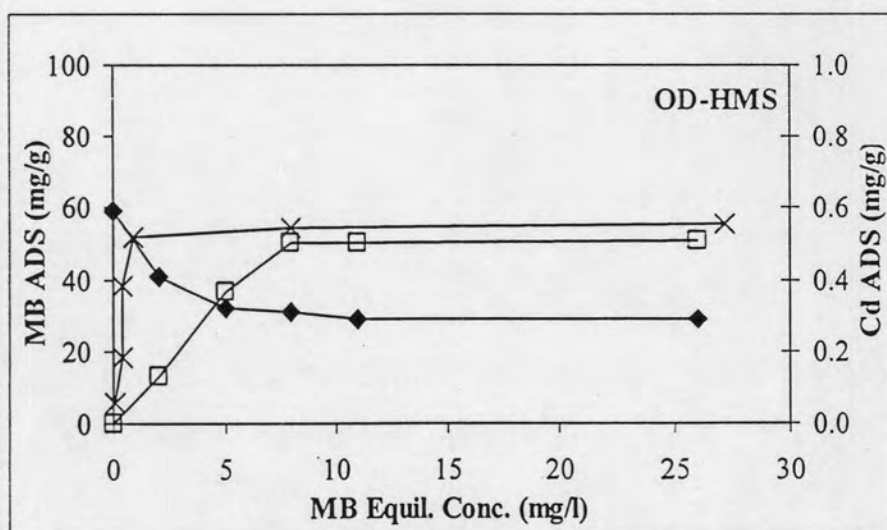

Figure 4.43 Adsorption capacity of MB on A-HMS by fixing initial Cd(II) concentration under mixing with various MB concentration at pH 5, Ionic strength 0.1 M and Temperature 25 °C: ♦, Cd(II) Bi-solute; □, MB Bi-solute; x, MB Single-solute.
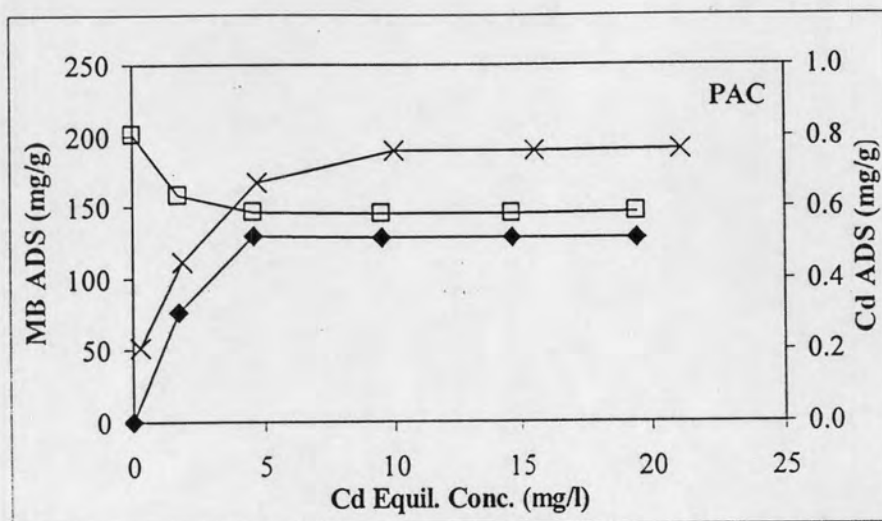
Figure 4.44 Adsorption capacity of Cd(II) on M-HMS by fixing initial MB concentration under mixing with various Cd(II) concentration at pH 5, Ionic strength 0.1 M, Temperature 25 °C: ♦, Cd(II) Bi-solute; □, MB Bi-solute; x, Cd(II) Single-solute.

Figure 4.45 Adsorption capacity of MB on M-HMS by fixing initial Cd(II) concentration under mixing with various MB concentration at pH 5, Ionic strength 0.1 M and Temperature 25 °C: ♦, Cd(II) Bi-solute; □, MB Bi-solute; x, MB Single-solute.

Figure 4.46 Adsorption capacity of Cd(II) on OD-HMS by fixing initial MB concentration under mixing with various Cd(II) concentration at pH 5, Ionic strength 0.1 M, Temperature 25 °C: ♦, Cd(II) Bi-solute; □, MB Bi-solute; x, Cd(II) Single-solute.
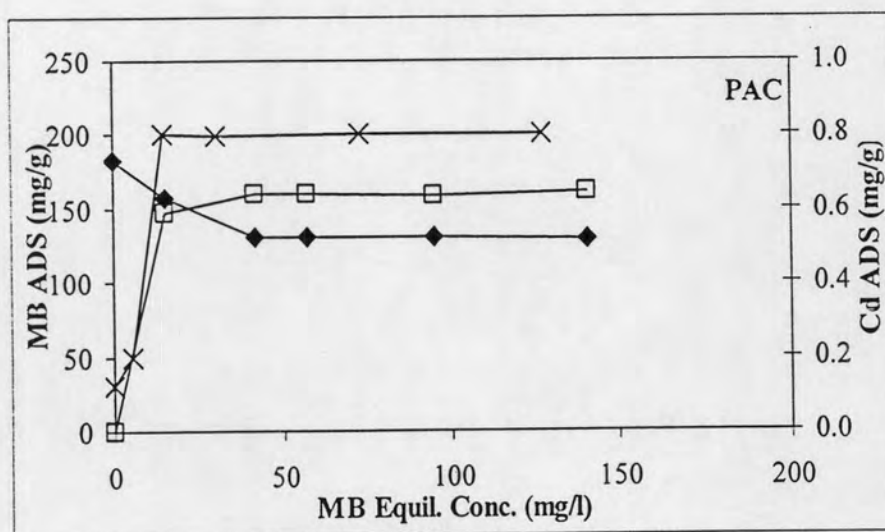

Figure 4.47 Adsorption capacity of MB on OD-HMS by fixing initial Cd(II) concentration under mixing with various MB concentration at pH 5, Ionic strength 0.1 M and Temperature 25 °C: ♦, Cd(II) Bi-solute; □, MB Bi-solute; x, MB Single-solute.

Figure 4.48 Adsorption capacity of Cd(II) on PAC by fixing initial MB concentration under mixing with various Cd(II) concentration at pH 5, Ionic strength 0.1 M, Temperature 25 °C: ♦, Cd(II) Bi-solute; □, MB Bi-solute; x, Cd(II) Single-solute.

Figure 4.49 Adsorption capacity of MB on PAC by fixing initial Cd(II) concentration under mixing with various MB concentration at pH 5, Ionic strength 0.1 M and Temperature 25 °C: ♦, Cd(II) Bi-solute; □, MB Bi-solute; x, MB Single-solute.

The adsorption isotherm of Cd(II) on HMS was decreased. Decrease of MB adsorption capacities on HMS can be detected by comparing with the single solution isotherm. The amount of Cd(II) adsorption capacities decreased from 0.51 to 0.35 mg/g. Moreover, the amount of MB adsorption capacities decreased from 36.23 to 32.61 mg/g.

The adsorption isotherm of Cd(II) on A-HMS was decreased. Decrease of MB adsorption capacities on A-HMS can be detected by comparing with the single solution isotherm. The amount of Cd(II) adsorption capacities decreased from 0.37 to 0.07 mg/g. Moreover, the amount of MB adsorption capacities decreased from 4.82 to 2.27 mg/g.

The adsorption isotherm of Cd(II) on M-HMS was decreased. Decrease of MB adsorption capacities on M-HMS can be detected by comparing with the single solution isotherm. The amount of Cd(II) adsorption capacities decreased from 2.91 to 2.53 mg/g. Moreover, the amount of MB adsorption capacities decreased from 47.26 to 40.29 mg/g.

The adsorption isotherm of Cd(II) on OD-HMS was decreased. Decrease of MB adsorption capacities on OD-HMS can be detected by comparing with the single solution isotherm. The amount of Cd(II) adsorption capacities decreased from 0.59 to 0.27 mg/g. Moreover, the amount of MB adsorption capacities decreased from 55.36 to 50.89 mg/g.

The adsorption isotherm of Cd(II) on PAC was decreased. Decrease of MB adsorption capacities on PAC can be detected by comparing with the single solution isotherm. The amount of Cd(II) adsorption capacities decreased from 0.73 to 0.51 mg/g. Moreover, the amount of MB adsorption capacities decreased from 200.40 to 161.68 mg/g.
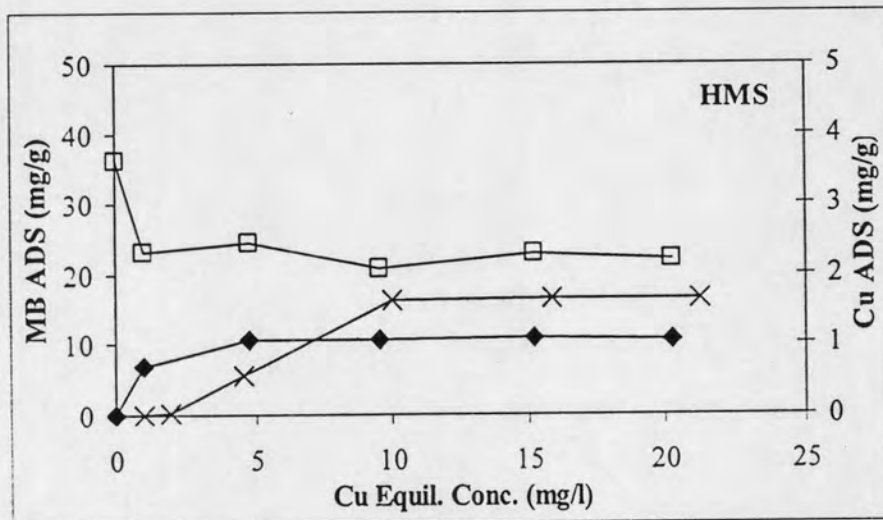
(b) Cu(II) and methylene blue

Figure 4.50 Adsorption capacity of Cu(II) on HMS by fixing initial MB concentration under mixing with various Cu(II) concentration at pH 5, Ionic strength 0.1 M, Temperature 25 °C: ♦, Cu(II) Bi-solute; □, MB Bi-solute; x, Cu(II) Single-solute.
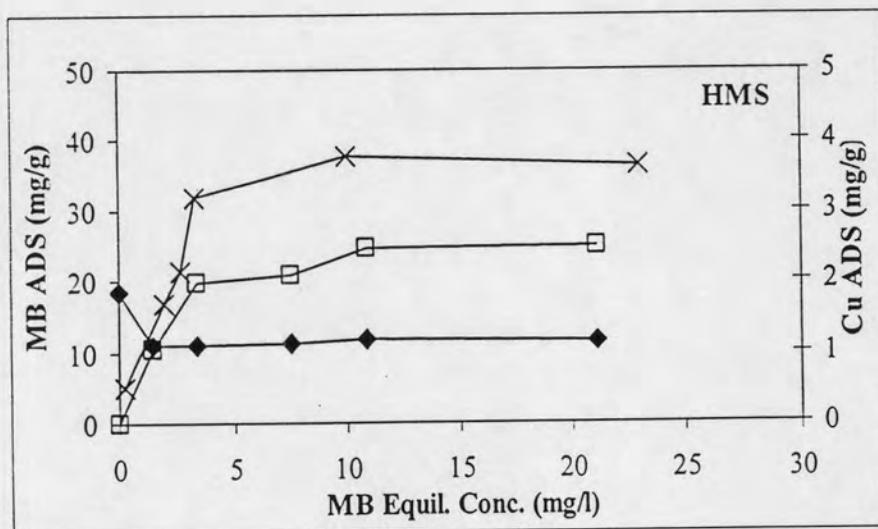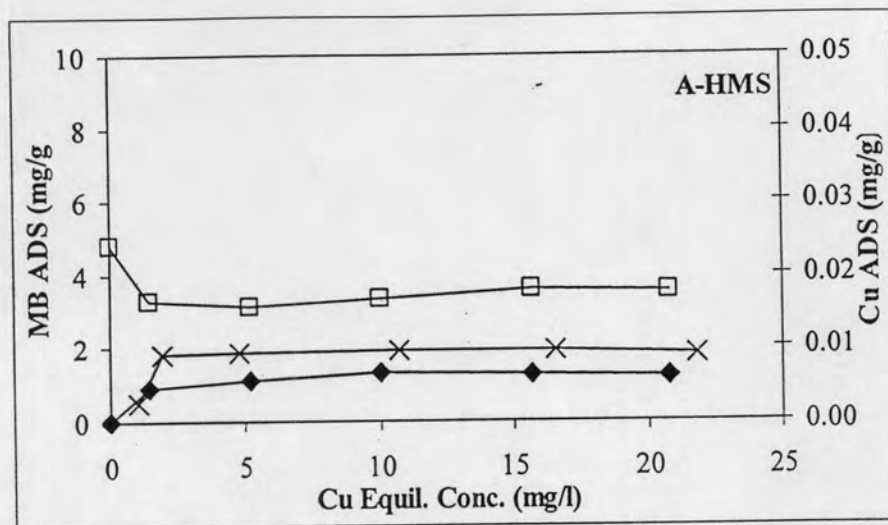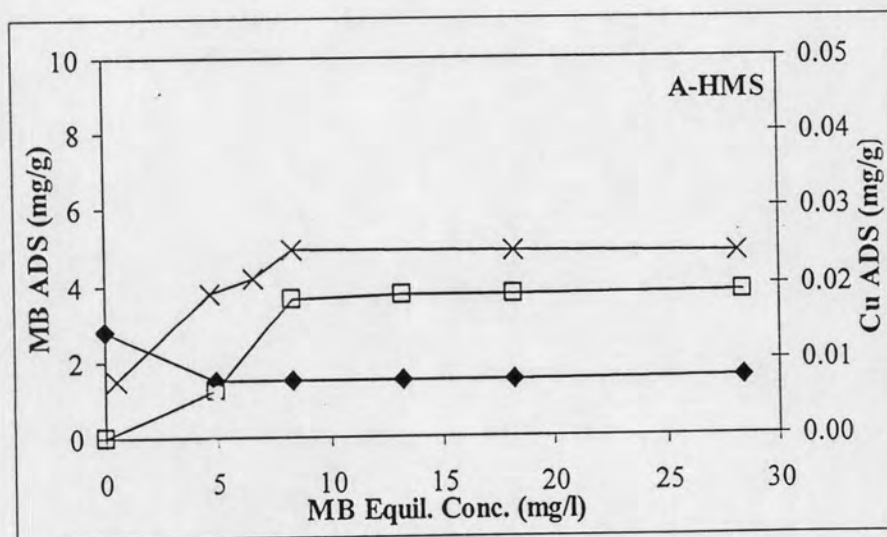

Figure 4.51 Adsorption capacity of MB on HMS by fixing initial Cu(II) concentration under mixing with various MB concentration at pH 5, Ionic strength 0.1 M and Temperature 25 °C: ♦, Cu(II) Bi-solute; □, MB Bi-solute; x, MB Single-solute.
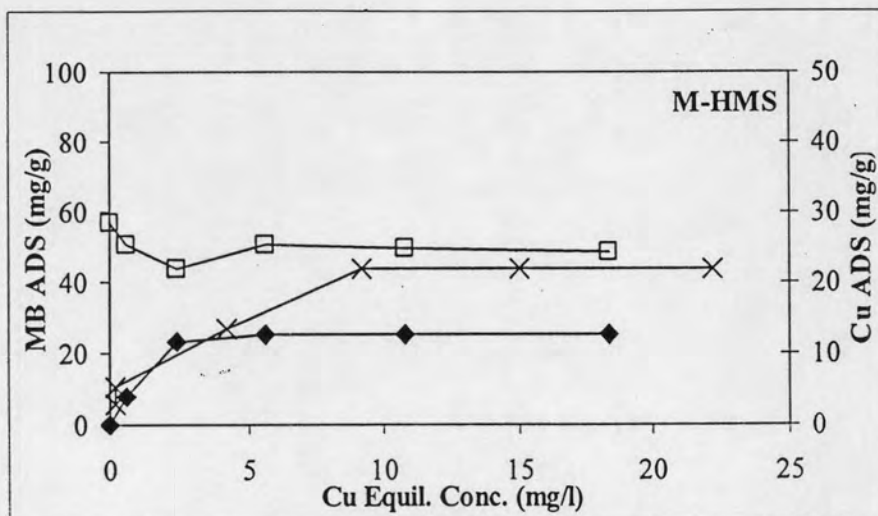
Figure 4.52 Adsorption capacity of Cu(II) on A-HMS by fixing initial MB concentration under mixing with various Cu(II) concentration at pH 5, Ionic strength 0.1 M, Temperature 25 °C: ♦, Cu(II) Bi-solute; □, MB Bi-solute; x, Cu(II) Single-solute.
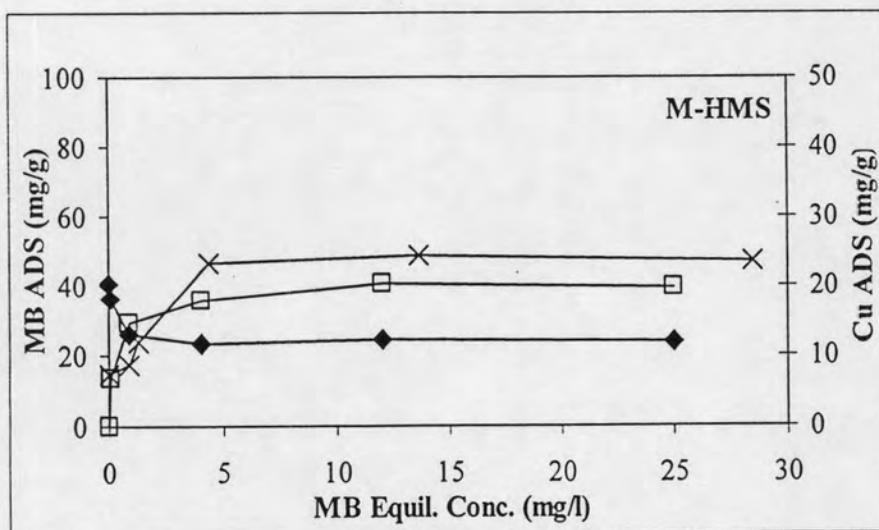

Figure 4.53 Adsorption capacity of MB on A-HMS by fixing initial Cu(II) concentration under mixing with various MB concentration at pH 5, Ionic strength 0.1 M and Temperature 25 °C: ♦, Cu(II) Bi-solute; □, MB Bi-solute; x, MB Single-solute.

Figure 4.54 Adsorption capacity of Cu(II) on M-HMS by fixing initial MB concentration under mixing with various Cu(II) concentration at pH 5, Ionic strength 0.1 M, Temperature 25 °C: ♦, Cu(II) Bi-solute; □, MB Bi-solute; x, Cu(II) Single-solute.

Figure 4.55 Adsorption capacity of MB on M-HMS by fixing initial Cu(II) concentration under mixing with various MB concentration at pH 5, Ionic strength 0.1 M and Temperature 25 °C: ♦, Cu(II) Bi-solute; □, MB Bi-solute; x, MB Single-solute.
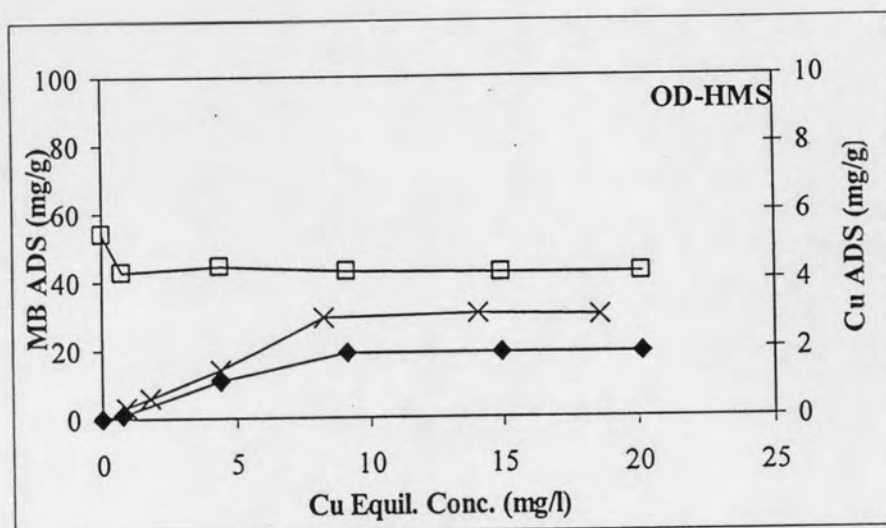
Figure 4.56 Adsorption capacity of Cu(II) on OD-HMS by fixing initial MB concentration under mixing with various Cu(II) concentration at pH 5, Ionic strength 0.1 M, Temperature 25 °C: ♦, Cu(II) Bi-solute; □, MB Bi-solute; x, Cu(II) Single-solute.
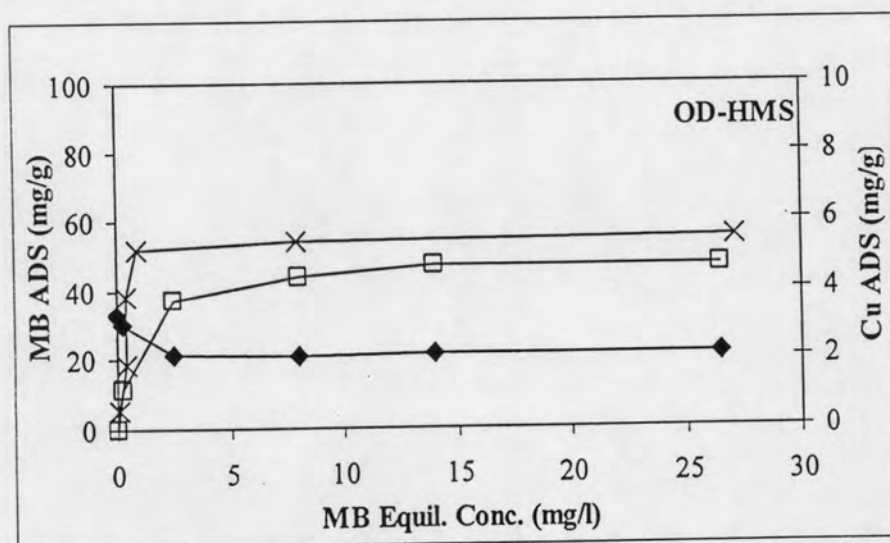

Figure 4.57 Adsorption capacity of MB on OD-HMS by fixing initial Cu(II) concentration under mixing with various MB concentration at pH 5, Ionic strength 0.1 M and Temperature 25 °C: ♦, Cu(II) Bi-solute; □, MB Bi-solute; x, MB Single-solute.
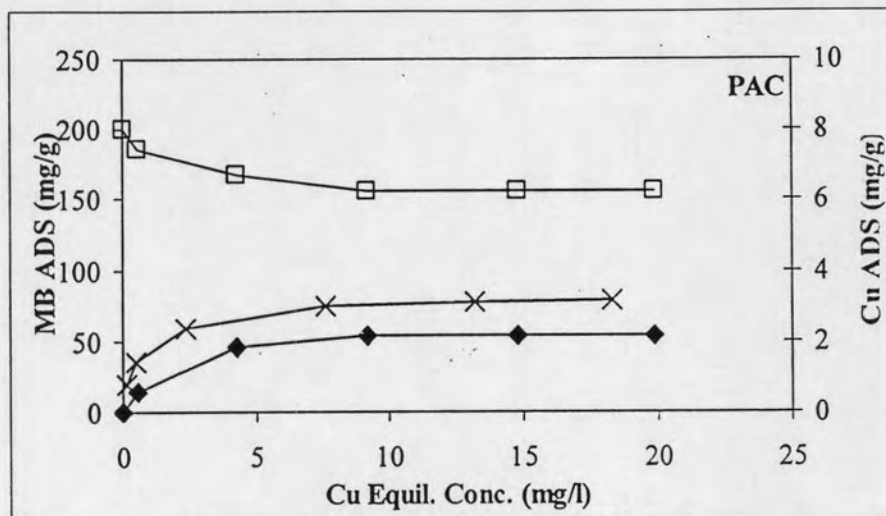
Figure 4.58 Adsorption capacity of Cu(II) on PAC by fixing initial MB concentration under mixing with various Cu(II) concentration at pH 5, Ionic strength 0.1 M, Temperature 25 °C: ♦, Cu(II) Bi-solute; □, MB Bi-solute; x, Cu(II) Single-solute.
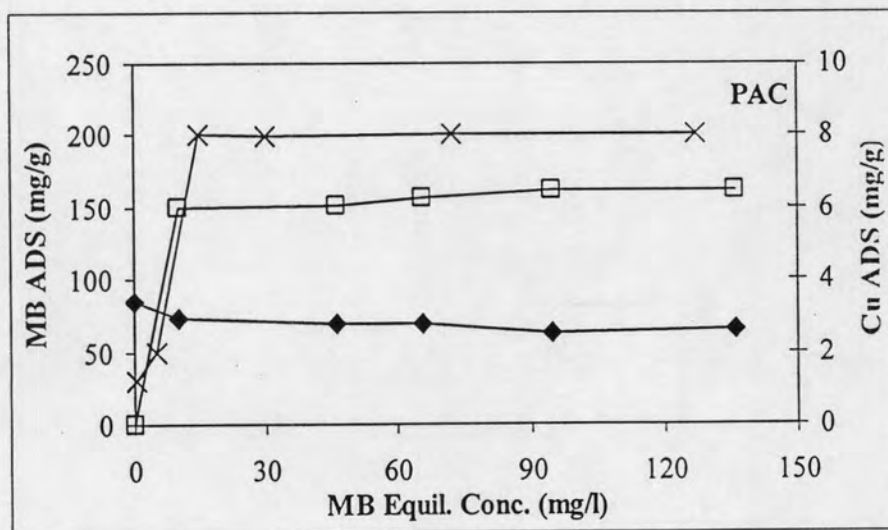

Figure 4.59 Adsorption capacity of MB on PAC by fixing initial Cu(II) concentration under mixing with various MB concentration at pH 5, Ionic strength 0.1 M and Temperature 25 °C: ♦, Cu(II) Bi-solute; □, MB Bi-solute; x, MB Single-solute.

The adsorption isotherm of Cu(II) on HMS was decreased. Decrease of MB adsorption capacities on HMS can be detected by comparing with the single solution isotherm. The amount of Cu(II) adsorption capacities decreased from 1.64 to 1.07 mg/g. Moreover, the amount of MB adsorption capacities decreased from 36.25 to 24.97 mg/g.

The adsorption isotherm of Cu(II) on A-HMS was decreased. Decrease of MB adsorption capacities on A-HMS can be detected by comparing with the single solution isotherm. The amount of Cu(II) adsorption capacities decreased from 0.01 to 0.005 mg/g. Moreover, the amount of MB adsorption capacities decreased from 4.81 to 2.26 mg/g.

The adsorption isotherm of Cu(II) on M-HMS was decreased. Decrease of MB adsorption capacities on M-HMS can be detected by comparing with the single solution isotherm. The amount of Cu(II) adsorption capacities decreased from 24.95 to 12.75 mg/g. Moreover, the amount of MB adsorption capacities decreased from 47.26 to 39.49 mg/g.

The adsorption isotherm of Cu(II) on OD-HMS was decreased. Decrease of MB adsorption capacities on OD-HMS can be detected by comparing with the single solution isotherm. The amount of Cu(II) adsorption capacities decreased from 2.91 to 1.91 mg/g. Moreover, the amount of MB adsorption capacities decreased from 55.36 to 46.76 mg/g.

The adsorption isotherm of Cu(II) on PAC was decreased. Decrease of MB adsorption capacities on PAC can be detected by comparing with the single solution isotherm. The amount of Cu(II) adsorption capacities decreased from 3.17 to 2.14 mg/g. Moreover, the amount of MB adsorption capacities decreased from 200.40 to 161.16 mg/g.

4.3.3.3 TX-100 and methylene blue

The adsorption isotherms in bi-solution between TX-100 and MB were shown in Figure 4.60-4.69. Effects of TX-100 on MB adsorption capacities were conducted at Tx-100 concentration from 50 to 600 mg/L and fixed concentration of MB at 30 mg/L, except PAC was fixed at 100 mg/L . Moreover, effect of MB on TX-100 adsorption capacities was also studied by mixing solution between fixed concentration of TX-100 at 600 mg/L and vary concentration of MB at 5-30 mg/L and 60-150 mg/L for all HMSs and PAC respectively. These results showed that the adsorption capacity of TX-100 increased, comparing with adsorption isotherms in single-solute, however, adsorption capacities of MB decreased for all of adsorbents. These changes also happened in the twist phase of bi-solute adsorption isotherms too. The order of the highest change of increased adsorption capacities for TX-100 was A-HMS > M-HMS > OD-HMS > PAC > HMS, with the percent increasing at 52.63%, 28.97%, 23.77%, 11.77% and 11.63%, respectively. However, for decreasing of MB adsorption capacities on A-HMS was highest for mixing with TX-100 at 93.54%.

However, according to Nunn *et al.* (1982), adsorption of sodium p-(1-propylnonyl)benzenesulfonate, an anionic surfactant, on silicate material was a little bit changed by the presence of dye (pinacynol chloride). In this study, all adsorption of MB decreased as the concentration of TX-100 increased. These results showed that adsorbed TX-100 on HMSs and PAC affected to active surface accessibility of MB. Adsorption capacities of MB decreased by more than 50% when less than a half of maximum adsorbable TX-100 was adsorbed (less than 200 mg/g of TX-100 adsorption). This result indicates that there are other effects of TX-100 adsorption than competition for active adsorption sites to interfere with MB adsorption. For example, the van der waals interaction between octyl functional groups of OD-HMS and MB is decreased by adsorption of TX-100. The interactions between ethoxylate chain or octylphenol part of TX-100 molecule, and the surfaces of HMSs and PAC are stronger than interaction of MB with HMSs and PAC, which cause decreasing of MB adsorption capacities on both hydrophilic and hydrophobic surfaces. In the case of PAC, adsorbed TX-100 can block the micropores, which reduces the effective surface area significantly.

Janos *et al.* (2003) reported that the adsorption of dyes was not affected by non-ionic surfactant or surfactant having the same charge as dyes. On the contrary, Zhu *et al.* (1998) reported increase of adsorption capacity of Chrome Azurol S (anionic dyes), which was caused by surface solubility. As shown in Figure 4.60-4.69 the adsorption of MB did not increase even the TX-100 concentration was raised to a concentration higher than cmc (143 mg/l). These results indicate that surface solubilization of MB on HMSs and PAC did not take place in these experiments.

However, adsorption capacities of TX-100 on all adsorbents in bi-solution were increased significantly. Presence of MB on surface might a little bit increase surface complexity of all surfaces that affect to adsorption capacities of TX-100.
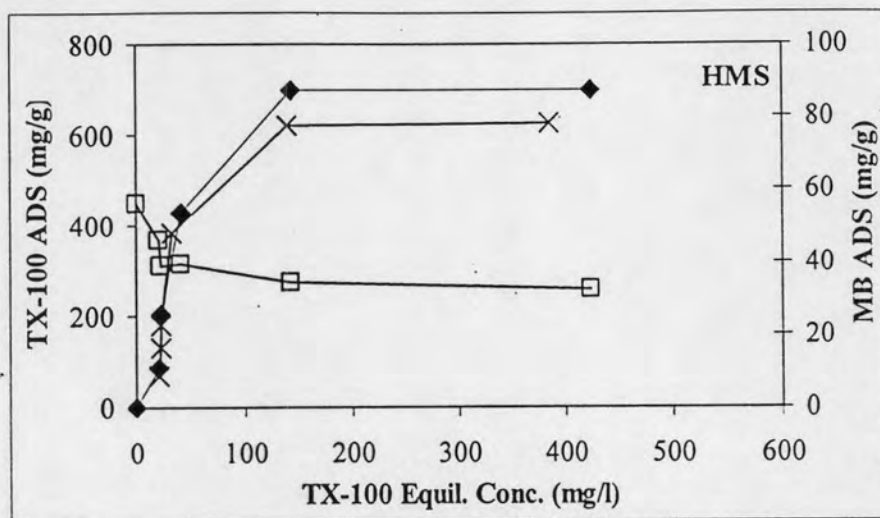
Figure 4.60 Adsorption capacity of TX-100 on HMS by fixing initial MB concentration under mixing with various TX-100 concentration at pH 5, Ionic strength 0.1 M, Temperature 25 °C: ♦, TX-100 Bi-solute; □, MB Bi-solute; x, TX-100 Single-solute.
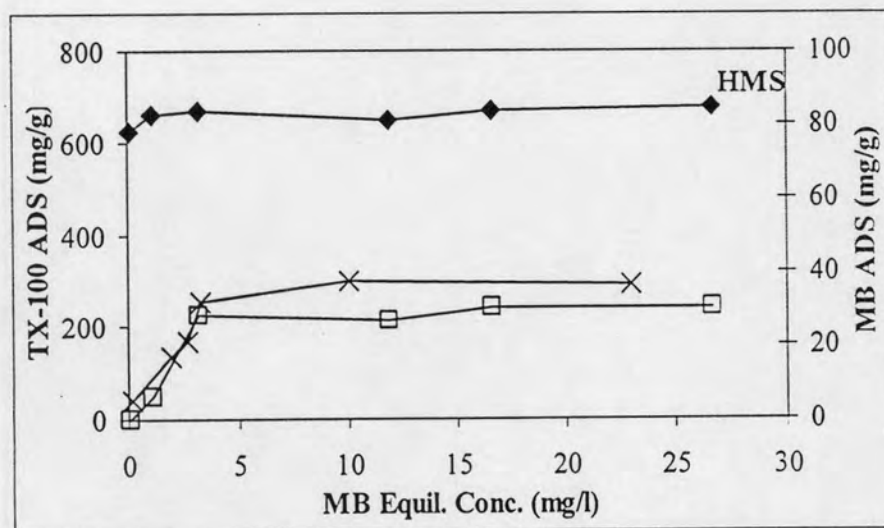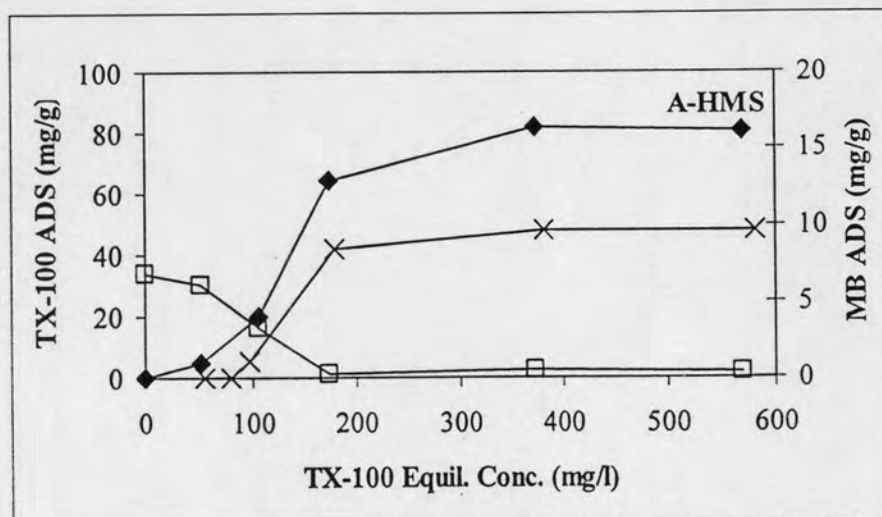

Figure 4.61 Adsorption capacity of MB on HMS by fixing initial TX-100 concentration under mixing with various MB concentration at pH 5, Ionic strength 0.1 M and Temperature 25 °C: ♦, TX-100 Bi-solute; □, MB Bi-solute; x, MB Single-solute.

Figure 4.62 Adsorption capacity of TX-100 on A-HMS by fixing initial MB concentration under mixing with various TX-100 concentration at pH 5, Ionic strength 0.1 M, Temperature 25 °C: ♦, TX-100 Bi-solute; □, MB Bi-solute; x, TX-100 Single-solute.
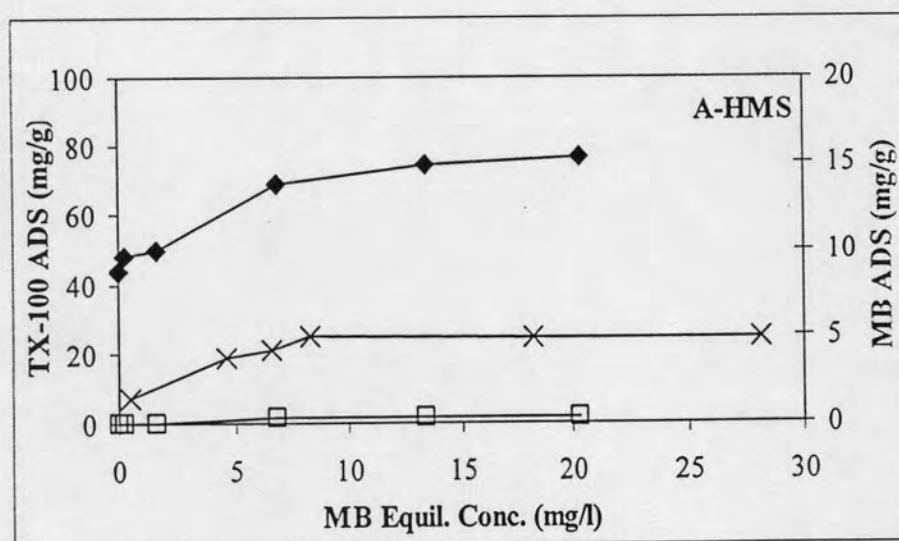

Figure 4.63 Adsorption capacity of MB on M-HMS by fixing initial TX-100 concentration under mixing with various MB concentration at pH 5, Ionic strength 0.1 M and Temperature 25 °C: ♦, TX-100 Bi-solute; □, MB Bi-solute; x, MB Single-solute.
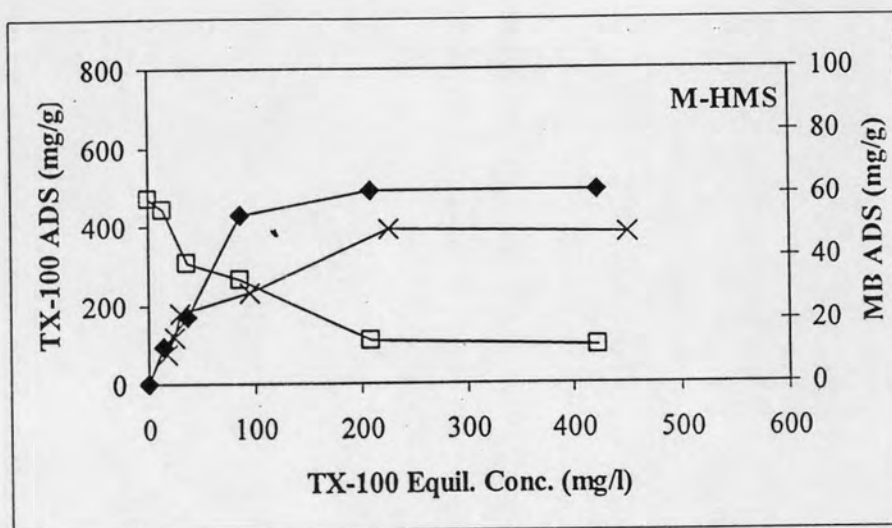
Figure 4.64 Adsorption capacity of TX-100 on HMS by fixing initial MB concentration under mixing with various TX-100 concentration at pH 5, Ionic strength 0.1 M, Temperature 25 °C: ♦, TX-100 Bi-solute; □, MB Bi-solute; x, TX-100 Single-solute.
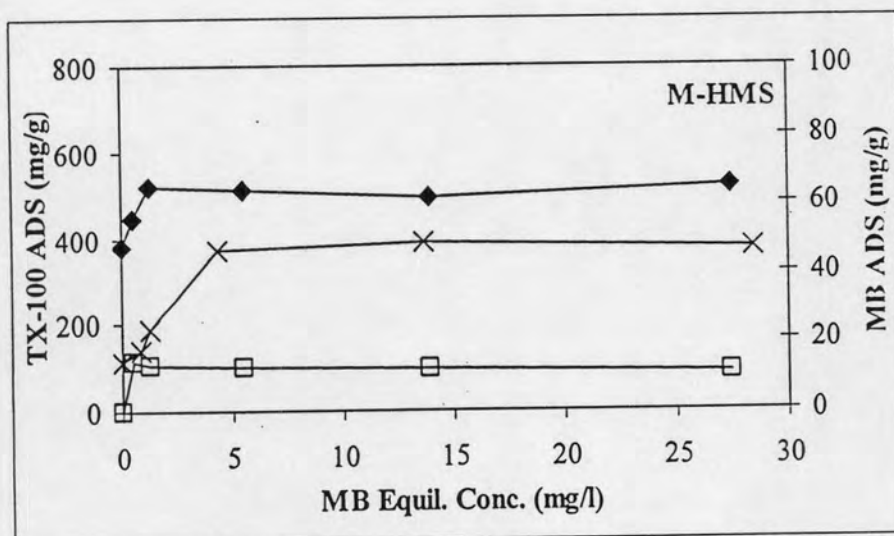

Figure 4.65 Adsorption capacity of MB on M-HMS by fixing initial TX-100 concentration under mixing with various MB concentration at pH 5, Ionic strength 0.1 M and Temperature 25 °C: ♦, TX-100 Bi-solute; □, MB Bi-solute; x, MB Single-solute.
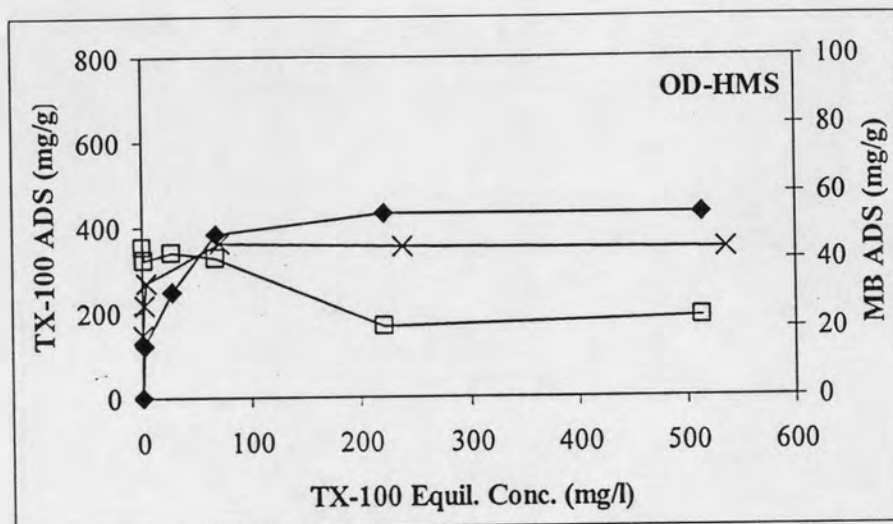
Figure 4.66 Adsorption capacity of TX-100 on OD-HMS by fixing initial MB concentration under mixing with various TX-100 concentration at pH 5, Ionic strength 0.1 M, Temperature 25 °C: ♦, TX-100 Bi-solute; □, MB Bi-solute; x, TX-100 Single-solute.
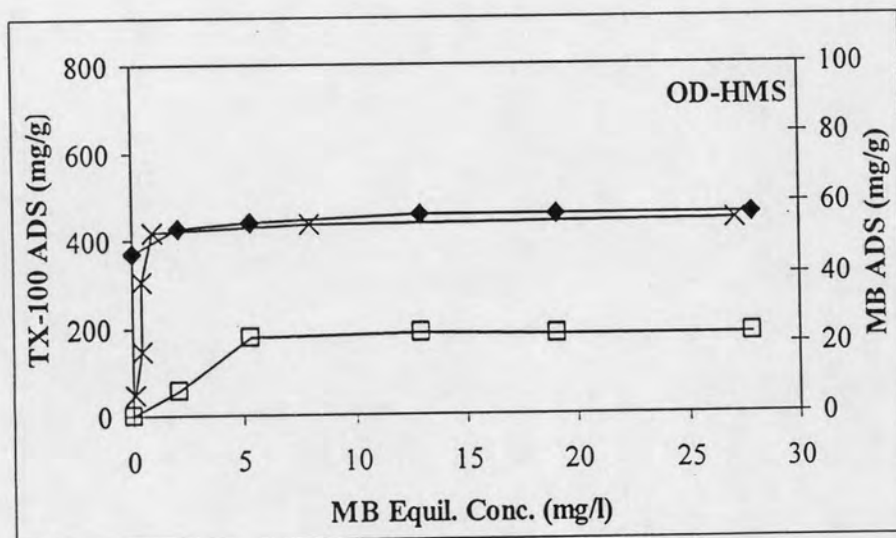

Figure 4.67 Adsorption capacity of MB on OD-HMS by fixing initial TX-100 concentration under mixing with various MB concentration at pH 5, Ionic strength 0.1 M and Temperature 25 °C: ♦, TX-100 Bi-solute; □, MB Bi-solute; x, MB Single-solute.

Figure 4.68 Adsorption capacity of TX-100 on PAC by fixing initial MB concentration under mixing with various TX-100 concentration at pH 5, Ionic strength 0.1 M, Temperature 25 °C: ♦, TX-100 Bi-solute; □, MB Bi-solute; x, TX-100 Single-solute.

Figure 4.69 Adsorption capacity of MB on PAC by fixing initial TX-100 concentration under mixing with various MB concentration at pH 5, Ionic strength 0.1 M and Temperature 25 °C: ♦, TX-100 Bi-solute; □, MB Bi-solute; x, MB Single-solute.
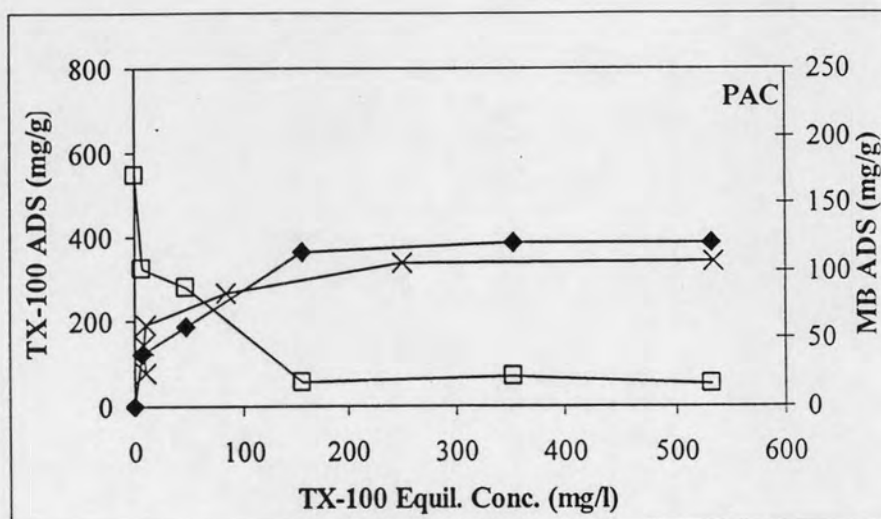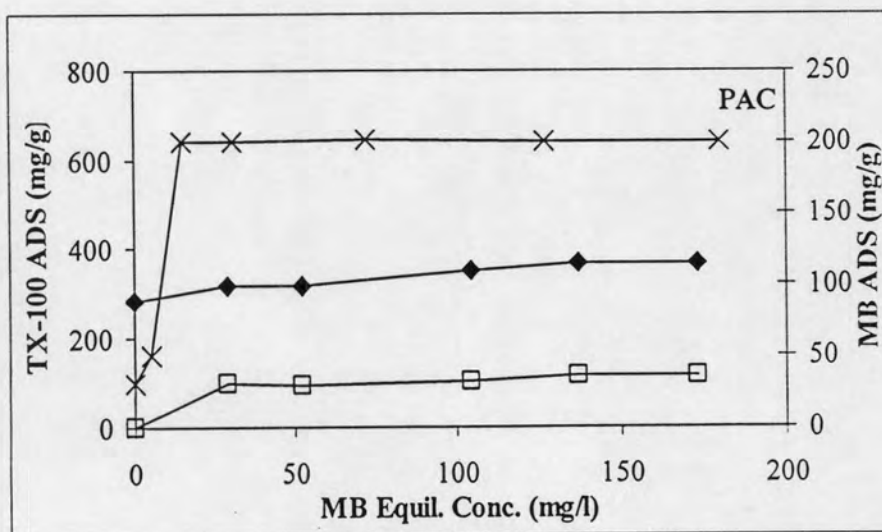
The adsorption isotherm of TX-100 on HMS was increased, on the other hand, the adsorption isotherm of MB on HMS was decreased, comparing with the single solution isotherms. This result indicated that adsorbed TX-100 covered active sites of HMS that decrease MB adsorption capacities. MB adsorption capacities decreased from 36.25 to 30.11 mg/g. However, TX-100 adsorption capacities increased from 625.58 to 698.32 mg/g.

The adsorption isotherm of TX-100 on A-HMS was increased, on the other hand, the adsorption isotherm of MB on A-HMS was decreased, comparing with the single solution isotherms. This result indicated that adsorbed TX-100 covered active sites of A-HMS that decrease MB adsorption capacities. MB adsorption capacities decreased from 4.82 to 0.31 mg/g. However, TX-100 adsorption capacities increased from 52.90 to 80.74 mg/g.

The adsorption isotherm of TX-100 on M-HMS was increased, on the other hand, the adsorption isotherm of MB on M-HMS was decreased, comparing with the single solution isotherms. This result indicated that adsorbed TX-100 covered active sites of M-HMS that decrease MB adsorption capacities. MB adsorption capacities decreased from 47.26 to 11.19 mg/g. However, TX-100 adsorption capacities increased from 381.11 to 491.54 mg/g.

The adsorption isotherm of TX-100 on OD-HMS was increased, on the other hand, the adsorption isotherm of MB on OD-HMS was decreased, comparing with the single solution isotherms. This result indicated that adsorbed TX-100 covered active sites of OD-HMS that decrease MB adsorption capacities. MB adsorption capacities decreased from 55.36 to 22.50 mg/g. However, TX-100 adsorption capacities increased from 348.72 to 431.59 mg/g.

The adsorption isotherm of TX-100 on PAC was increased, on the other hand, the adsorption isotherm of MB on PAC was decreased, comparing with the single solution isotherms. This result indicated that adsorbed TX-100 covered active sites of PAC that decrease MB adsorption capacities. MB adsorption capacities decreased from 200.40 to 34.99 mg/g. However, TX-100 adsorption capacities increased from 342.45 to 382.76 mg/g.